



HAL
open science

Migration of Reversing Dunes Against the Sand Flow Path as a Singular Expression of the Speed Up Effect

Xin Gao, Clément Narteau, Cyril Gadal

► **To cite this version:**

Xin Gao, Clément Narteau, Cyril Gadal. Migration of Reversing Dunes Against the Sand Flow Path as a Singular Expression of the Speed Up Effect. *Journal of Geophysical Research: Earth Surface*, 2021, 126, 19 pp. 10.1029/2020JF005913 . insu-03590051

HAL Id: insu-03590051

<https://insu.hal.science/insu-03590051>

Submitted on 3 Mar 2022

HAL is a multi-disciplinary open access archive for the deposit and dissemination of scientific research documents, whether they are published or not. The documents may come from teaching and research institutions in France or abroad, or from public or private research centers.

L'archive ouverte pluridisciplinaire **HAL**, est destinée au dépôt et à la diffusion de documents scientifiques de niveau recherche, publiés ou non, émanant des établissements d'enseignement et de recherche français ou étrangers, des laboratoires publics ou privés.

Copyright

JGR Earth Surface

RESEARCH ARTICLE

10.1029/2020JF005913

Key Points:

- Reversing dunes can migrate against the resultant drift direction
- Speed-up effect and frequent wind reversals explain the dune migration paradox
- Daily and storm cycles illustrate the control of wind sequence on dune dynamics

Correspondence to:

X. Gao,
gaoxin@ms.xjb.ac.cn

Citation:

Gao, X., Narteau, C., & Gadal, C. (2021). Migration of reversing dunes against the sand flow path as a singular expression of the speed-up effect. *Journal of Geophysical Research: Earth Surface*, 126, e2020JF005913. <https://doi.org/10.1029/2020JF005913>

Received 22 SEP 2020
Accepted 26 MAR 2021

Migration of Reversing Dunes Against the Sand Flow Path as a Singular Expression of the Speed-Up Effect

Xin Gao^{1,2} , Clément Narteau³ , and Cyril Gadal³ 

¹State Key Laboratory of Desert and Oasis Ecology, Xinjiang Institute of Ecology and Geography, Chinese Academy of Sciences, Xinjiang, China, ²University of Chinese Academy of Sciences, Beijing, China, ³Institut de Physique du Globe de Paris, Université de Paris, CNRS, Paris, France

Abstract We study the morphodynamics of reversing dunes on the gravel deposits of the alluvial fan of the Molcha river at the border between the Tibetan Plateau and the Taklamakan Desert. Independent sets of wind data show that this area of low sand availability is exposed to two prevailing winds from opposite directions and of different strengths. The predicted resultant transport direction of sand particles is westward. Nevertheless, satellite observations combined with field measurements and ground-penetrating radar surveys reveal that isolated dunes a few meters high migrate eastward. This apparent dune migration paradox is resolved using numerical and analytical models that take into account the speed-up effect and the continuous change in dune shape after each wind reversal. When a newly established wind hits what was before the steeper lee slope of the dune, the sand flux at the crest abruptly increases before relaxing back to a constant value as the crest migrates downwind and as the dune reaches a new steady shape. Integrated over the entire wind cycle, we find that this non-linear behavior causes reversing dunes to migrate against the resultant transport direction. This migration reflects the difference in dune slope seen by irregular storm events blowing to the east and the westward wind of the daily cycle. Thus, we explore the impact of extreme events on dune morphodynamics and examine new aspects of the permanent feedback between dune topography and wind speed. We conclude that transient behaviors associated with crest reversals contribute to the observed diversity of dune patterns, even within the same area for dunes of different sizes.

Plain Language Summary The wind accelerates when it is deflected over a dune so that the sand flux at the crest is several times greater than on a flat sand bed far from any topography. This speed-up effect varies as the steepness of the dune slopes exposed to the wind. Here we show that, in zones of frequent wind reversals, the speed-up effect can cause the dunes to migrate against the transport direction of windblown sand particles. This apparent dune migration paradox requires specific conditions which are met in the study area, a large (8,000 km²) alluvial fan at the margin between the Tibetan Plateau and the Taklamakan Desert. First, it is an area of low sand availability and the dunes that develop on the gravel deposits of the alluvial fan do not exceed a few meters in height. Second, this area is submitted to two opposite winds with different strengths. Westward winds are weak but occur daily, while eastward winds are associated with storm events. Since the infrequent storm winds always blow over a dune that is regularly smoothed by daily winds from the opposite direction, they produce much greater sand flux at the crest of the so-called reversing dunes, which can then migrate against the sand flow path. This singular behavior governed by the permanent feedback between airflow and dune topography illustrates the critical role of extreme events in sediment transport dynamics.

1. Introduction

Reversing dunes are usually recognized by their linear shapes and transverse orientation in regions, where two prevailing winds blow from opposite directions (McKee, 1966; Merk, 1960). As the wind blows alternately from both sides of their crest, they form from crest reversals that successively rework former lee slopes and generate new slip faces on former stoss slopes. In major sand seas, reversing dunes can grow to giant size together with star dunes (Andreotti et al., 2009). Since the main directions of sediment transport cancel each other out, these giant dunes have extremely low rates of migration. Where they are large enough not to be completely reshaped by a seasonal wind, reversing dunes can be easily identified, thanks to their symmetrical shape and the steep slopes on either side of their long linear ridges (Z. Dong et al., 2009; McKee, 1979). Smaller scale reversing dunes are also often reported in different environments on Earth and other planetary bodies as soon as bed forms grow under the combined effect of two dominant winds responsible for frequent crest reversals (Bristow et al., 2010;

Burkinshaw & Rust, 1993; Dluzewski & Rotnicka, 2019; Y. Dong et al., 2017; Jackson et al., 2020; Lorenz & Zimbelman, 2014; Neuman et al., 1997; Rockett et al., 2016; Walker, 1999). Nevertheless, the morphodynamics of reversing dunes has not been the subject of extensive research and the impact of changes in wind directionality on the steepness of dune slopes remains so far poorly documented.

Despite the variety of possible multidirectional wind regimes, those characterized by two prevailing winds blowing from opposite directions are frequently observed on Earth due to the seasonality of near-surface atmospheric flows and/or the influence of local topography. In dune studies, these specific wind regimes are regarded as singularities, especially when the two winds tend to have the same transport capacity. In this case, the resultant sand flux tends to 0, and as its direction is highly sensitive to small variations in wind strength and orientation, it can no longer be used as a reference to measure the dune alignment (Hunter et al., 1983; Ping et al., 2014; Rubin & Hunter, 1987). These small variations can also produce abrupt changes in dune shape, for example, from long linear dunes to trains of asymmetric barchans in zones of limited sand supply (Gao, Narteau, Rozier, Courrech du Pont, 2015). Then, given the natural variability of surface winds, dune fields experiencing opposite winds are expected to exhibit different types of dunes.

Compared to giant reversing dunes in major sand seas, less attention has been given to reversing dunes in zones of low sand availability, where dunes can also elongate thanks to the deposition at the tip of the sediment transported along the crest (Courrech du Pont et al., 2014; Lucas et al., 2015; Rozier et al., 2019). This dune growth mechanism only prevails in multidirectional wind regimes because it relies entirely on crest reversal, more exactly on the balance between the normal-to-crest components of transport coming from both sides of the crest. Hence, the theoretical formalism as well as the numerical, experimental, and field observations that have recently been gathered on elongating dunes provide a solid basis for the analysis of the morphodynamics of reversing dunes (Courrech du Pont et al., 2014; Gadal et al., 2020; Gao, Narteau, Rozier, Courrech du Pont, 2015; Lü et al., 2018; Nakao-Kusune et al., 2020; Zhang et al., 2012). Here, we take advantage of these results to study meter-high reversing dunes evolving on a nonerodible bed and to further explore the effect of the sequence of winds on dune shape and migration.

A positive topography deflects the air flow and the compression of streamlines causes the wind speed measured at a given height above the ground to be stronger on the stoss slope of an obstacle than on a flat bed away from any topography. Thus, there is a positive feedback between shear velocity and topography, so that the sand flux over a dune depends on its shape. Usually defined as the speed-up effect, this is a critical ingredient at all stages of the development of dunes, from the formation of incipient bedforms to the dynamics of major dune systems. The speed-up factor $u_{\text{crest}}/u_{\text{flat}}$ is the ratio between the wind speeds measured at the same height at the dune crest and on a flat bed away from any topography. It can also be expressed as

$$u_{\text{crest}} = u_{\text{flat}}(1 + \delta), \quad (1)$$

where $\delta \geq 0$ is the fractional speed-up ratio. Analyzing the theoretical response of a turbulent air flow to the perturbation induced by a symmetric hump with small curvature, Jackson and Hunt (1975) have shown that

$$\delta = \beta \frac{\mathcal{H}}{\mathcal{L}}, \quad (2)$$

where \mathcal{L} and \mathcal{H} are the characteristic length and height of the obstacle, and β a dimensionless coefficient that takes into account other physical ingredients (e.g., roughness) affecting surface wind speed (Britter et al., 1981). Based on Equation 2, the fractional speed-up ratio on a dune is usually considered to be directly proportional to its aspect ratio. This positive dependence of the speed up on dune aspect ratio has been observed on reversing dunes by Neuman et al. (1997). They report δ -values ranging from 0.5 to 2.5, in agreement with the values measured so far on different types of dunes around the world (Arens et al., 1995; Claudin et al., 2013; Walker & Nickling, 2003; Walker et al., 2009; Wiggs et al., 1996).

The speed-up correction is essential under unidirectional wind regimes to assess the dune migration rate (Zhang et al., 2010). It is even more crucial in multidirectional wind regimes to estimate the magnitude and the direction of the resultant flux at the crest. Since the apparent aspect ratio of dunes depends on the incident wind direction, the integrated transport at the crest differs from that over a flat sand bed not only in intensity, but also in direction. This dependence of the resultant sand flux on topography naturally explains the coexistence of different types of

dunes with various orientations (Courrech du Pont et al., 2014; Lü et al., 2018; Zhang et al., 2012). For reversing dunes, considering two winds with opposite directions blowing perpendicularly to the crest, this effect is all the more important as the apparent aspect ratio of the dune is maximal.

The remainder of this study is organized as follows. Section 2 provides a description of the wind data and the methods we use to predict sand fluxes and dune properties. It also presents the satellite and field measurement techniques from which we estimate dune migration. All our results on sediment transport and dune morphodynamics are exposed in Section 3, with respect to the characteristics of the local wind regime. We identify that the observed direction of dune migration is opposite to the resultant sand flux predicted from wind data. In Section 4, we show how the speed-up effect and the changes in dune shape after each wind reversal can resolve this dune migration paradox. The implications of these results are discussed in Section 5, as well as the impact of the wind sequence on dune morphodynamics.

2. Methods

The study area is located at the southern rim of the Taklamakan Desert on the large (8,000 km²) alluvial fan of the Molcha River flowing from the Altyn-Tagh mountains at the northern edge of the Tibetan Plateau (Figure 1a). This region exhibits complex dune fields composed of a variety of giant structures (≥ 100 m in height), including star, linear, and barchan dunes with superimposed bed forms. All these dunes migrate to the southwest up the slopes of the alluvial fan. The avulsion of the Molcha river and the successive flooding episodes have established a clear boundary between the area of high sand availability, where the giant dunes develop and the coarse alluvial fan deposits on which smaller dunes can be observed.

We focus here on these small dunes that form on the downstream border of the alluvial fan under conditions of limited sediment supply (Figure 1b). There, periodic dune patterns develop from thin layers of sand left behind by floods (Figure 1c). In between, isolated dunes also form as a result of grain-size segregation (Gao et al., 2016). All these dunes of metric height migrate with west-facing slip faces on the armored surface of the alluvial fan (Figures 1d and 1e).

2.1. Surface Wind Data

We use the 10 m surface wind data from the ECMWF ERA5 reanalysis (Hersbach et al., 2019). This global meteorological forecasting model based on assimilation aims to include all available and appropriate observational data from weather station, radiosonde, ship, and satellite measurements. It provides numerical predictions from the beginning of 1979 up to now with a horizontal spatial resolution of $0.25^\circ \times 0.25^\circ$ (about 28 km on the equator) and a time resolution of 1 h. The geographical coordinates of the ERA5 data analyzed here are 84.5°E and 37.5°N . The wind regime at this location is representative of the wind regime over the whole alluvial fan, which exhibits a gentle slope of 1° ($\approx 1.6\%$) and a low surface roughness in comparison to neighboring mountains and giant dune fields. We limit our analysis to the period from the beginning of 1990 to the end of 2019 because we observe an abrupt change in the wind regime in 1989, which could be associated with a change in the assimilation process (e.g., more local data available). This 30-year period is sufficient for our analysis because it is one order of magnitude longer than the characteristic time scales involved in the dynamics of the metric dunes we study.

To complete this numerical set of data by local observations, we have installed a wind tower on the gravel bed of the reversing dune field (Figure 1e). It has recorded both wind speed and direction at a height of 6 m with a time step of 1 min from April 24, 2018 to June 13, 2019. Over this time period, we can directly compare the ERA5 data with our local wind measurements.

2.2. From Wind Data to Sand Fluxes and Dune Properties

Wind data are used to compute sand fluxes and a set of variables relevant for dune morphodynamics. Table 1 shows the results obtained from the following formulae.

2.2.1. Saturated Sand Flux on a Flat Sand Bed

Wind measurements provide the wind speed u_i and direction θ_i at a height z and at different times t_i , $i \in [1; M]$. The shear velocity can be extrapolated using the law of the wall,

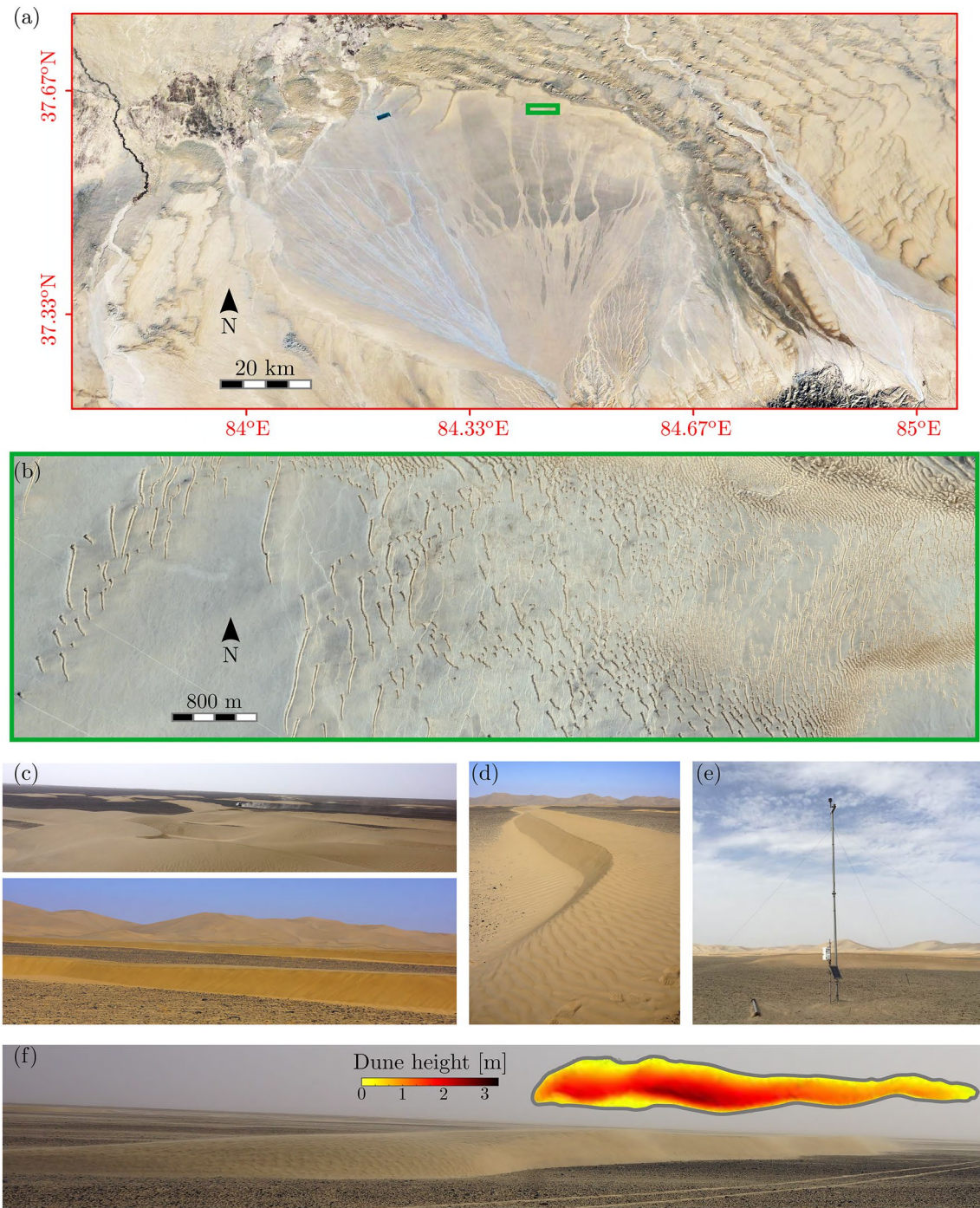


Figure 1. Reversing dunes at the northern edge of the Tibetan Plateau, China. (a) Location of the reversing dune field (green square) downstream of an alluvial fan where floods have stopped the migration of giant dunes from the southern margin of the Taklamakan Desert. (b) Zoom in on the reversing dune field. (c) Views taken from the reversing dune field. Dark interdunes are covered by gravel deposits that cannot be transported by the wind. Giant dunes in the background are to the east (bottom). (d) Typical section of a linear dune a few hundred meters long with a west-facing slip face. (e) Local wind tower installed in April 2018 (84.43°E, 37.65°N). (f) Morphology and topography of a 50 m long reversing dune. Car tracks give scale and show the armoring of the interdune areas (Gao et al., 2016).

Table 1
Shear Velocity, Sand Fluxes and Dune Orientations Derived From Wind data

| Variable | Units | Value | |
|--|-----------------------------|--|------------------------------|
| Acceleration of gravity g | m s^{-2} | 9.81 | |
| Grain size d | m | 180×10^{-6} | |
| Air density ρ_f | kg m^{-3} | 1.29 | |
| Grain density ρ_s | kg m^{-3} | 2.55×10^3 | |
| Aerodynamic roughness z_s | m | 10^{-3} | |
| von-Kármán constant κ | \emptyset | 0.4 | |
| Threshold shear velocity u_c | m s^{-1} | 0.19 | |
| | | Local wind tower 23/04/2018 → 13/06/2019 | ERA5 01/01/1990 → 31/12/2019 |
| Shear velocity and sand flux on a flat sand bed | | | |
| Mean shear velocity $\langle u_* \rangle$ | m s^{-1} | 0.29 | 0.25 |
| $\langle u_* \rangle / u_c$ | \emptyset | 1.5 | 1.34 |
| DP = $\langle \ \bar{Q}\ \rangle$ | $\text{m}^2 \text{yr}^{-1}$ | 47.9 | 16.9 |
| RDP = $\ \langle \bar{Q} \rangle\ $ | $\text{m}^2 \text{yr}^{-1}$ | 6.4 | 2.7 |
| RDP/DP | \emptyset | 0.13 | 0.16 |
| RDD | mod 360° | 190.1 | 246.0 |
| Dune orientation and sand flux at the crest | | | |
| Dune orientation α_i | mod 180° | 120.3 | 124.9 |
| Dune orientation α_F | mod 360° | 180.6 | 262.1 |
| $\ \langle \bar{Q}_i \rangle\ $ | $\text{m}^2 \text{yr}^{-1}$ | 16.9 | 7.7 |
| $\ \langle \bar{Q}_F \rangle\ $ | $\text{m}^2 \text{yr}^{-1}$ | 11.7 | 5.1 |
| Direction of $\langle \bar{Q}_i \rangle, \theta_{\bar{Q}_i}$ | mod 360° | 200.4 | 245.1 |

All angles are measured counterclockwise from east. The wind speed-up has been computed with $\gamma = 1.6$ (Gao, Narteau, Rozier, Courrech du Pont, 2015). Predicted dune orientations $\alpha_{(I,F)}$ show variation of 10° with respect to the γ -value. $\langle \bar{Q}_{(I,F)} \rangle$ are the mean sand fluxes at the crest of dunes aligned in the directions $\alpha_{(I,F)}$ of the bed instability and elongating modes, respectively (Courrech du Pont et al., 2014). DP, drift potential; RDD, resultant drift direction; RDP, resultant drift potential

$$u_*^i = \frac{u_i \kappa}{\log(z / z_s)}, \quad (3)$$

where κ is the von-Kármán constant. Instead of the geometric roughness that depends only on grain size, we consider here the aerodynamic roughness z_s that accounts for the height of the transport layer in which saltating grains modify the vertical wind velocity profile. The value of the threshold shear velocity for motion inception is determined using the formula calibrated by Iversen and Rasmussen (1999):

$$u_c = 0.1 \sqrt{\frac{\rho_s}{\rho_f} g d}, \quad (4)$$

where g is the gravitational acceleration, ρ_s / ρ_f the grain to fluid density ratio, and d the grain diameter (Table 1). The mean shear velocity $\langle u_* \rangle$ is defined as the shear velocity averaged over the transport periods, that is, when $Q_{\text{sat}} > 0$:

$$\langle u_* \rangle = \frac{1}{N} \sum_{i=1}^N u_*^i H_u^i \quad \text{where} \quad H_u^i = \begin{cases} 1 & \text{for } u_*^i > u_c, \\ 0 & \text{else.} \end{cases} \quad (5)$$

The saturated sand flux Q_{flat} on a flat sand bed is computed from the relationship proposed by Ungar and Haff (1987) and calibrated by Durán et al. (2011)

$$Q_{\text{flat}}(u_*) = \begin{cases} 25 \frac{\rho_r}{\rho_s} \sqrt{\frac{d}{g}} (u_*^2 - u_c^2) & \text{for } u_* > u_c, \\ 0 & \text{else.} \end{cases} \quad (6)$$

In this formula, the prefactor takes into account a dune compactness of 0.6. From the average of the individual saturated sand flux vectors \vec{Q}_{flat}^i , we estimate the resultant sand flux on a flat erodible bed:

$$\langle \vec{Q} \rangle = \frac{1}{N} \sum_{i=1}^N \vec{Q}_{\text{flat}}^i. \quad (7)$$

According to Fryberger and Dean (1979), the norm and direction of $\langle \vec{Q} \rangle$ are usually called the resultant drift potential (RDP) and the resultant drift direction (RDD), respectively. The latter is also referred to as the resultant transport direction. These two quantities are highly dependent on the wind directionality because the contributions of winds from opposite directions cancel each other out. For the entire time period, we also calculate the drift potential.

$$\text{DP} = \frac{1}{N} \sum_{i=1}^N \left\| \vec{Q}_{\text{flat}}^i \right\|. \quad (8)$$

Unlike the resultant drift potential, this mean sand flux does not take into account the orientation of the individual sand fluxes computed from the successive wind measurements. The ratio RDP/DP is a nondimensional parameter, which is often used to characterize the directional variability of the wind regimes (Fryberger & Dean, 1979; Pearce & Walker, 2005): RDP/DP \rightarrow 1 indicates that sand transport tends to be unidirectional; RDP/DP \rightarrow 0 indicates that most of the transport components cancel each other out.

2.2.2. Sand Flux at the Crest of Dunes

In the limit of strong winds, $u_* \gg u_c$, Equation 6 gives $Q_{\text{flat}} \propto u_*^2$. Then, the linear theory of Jackson and Hunt (1975) can be expanded to the sand flux at the first order of the dune aspect ratio. As for the wind speed in Equation 1, the sand flux at the crest can be expressed as

$$\vec{Q}_{\text{crest}} = \vec{Q}_{\text{flat}} (1 + 2\delta). \quad (9)$$

To compute these sand fluxes for all wind directions θ and all crest orientations α , Courrech du Pont et al. (2014) consider an infinite linear dune of constant shape of width W and height H . Then, $H|\sin(\theta - \alpha)|/W$ is the apparent aspect ratio of the dune, and

$$\vec{Q}_{\text{crest}} = \vec{Q}_{\text{flat}} \left(1 + \gamma |\sin(\theta - \alpha)| \right), \quad \text{where} \quad \gamma = 2\beta \frac{H}{W}. \quad (10)$$

This expression of \vec{Q}_{crest} is only valid for a symmetric linear dune of constant shape. It does not take into account the change in dune shape after each wind reversal (i.e., no crest reversal) nor a difference in slope between both sides of the dune.

2.2.3. Dune Orientations

According to our definition (Equation 10), the sand flux at the crest is a horizontal vector that can be decomposed into a normal-to-crest and a parallel-to-crest components of transport to predict dune orientation (see Figure 2 in Fernandez-Cascales et al., (2018)).

In zones with no limit in sand availability, dune growth is governed by the flat bed instability (Gadal et al., 2019). Under such transport-limited conditions, periodic dune patterns increase in amplitude perpendicularly to the direction for which the normal-to-crest component of transport is maximum (Rubin & Hunter, 1987). In practice, we calculate Q_{\perp} , the normal-to-crest component of transport for each time step i of the wind data and all crest orientations $\alpha \in [0; \pi]$. The orientation α_1 for which $\sum_i |Q_{\perp}^i|$ reaches a maximum determines the alignment of dunes in the bed instability mode. This procedure is also known as the gross bedform-normal transport rule, except that we take into account the speed-up effect. According to Equations 7 and 10, the resultant sand flux at the crest of dunes in the bed instability mode is

$$\langle \bar{Q}_1 \rangle = \frac{1}{N} \sum_{i=1}^N \bar{Q}_{\text{flat}}^i \left(1 + \gamma \left| \sin(\theta_i - \alpha_1) \right| \right). \quad (11)$$

Its orientation and magnitude give the direction and rate of dune migration.

In zones with low sand availability under multidirectional wind regimes, dunes can elongate in the direction of the resultant sand flux at the crest (Courrech du Pont et al., 2014; Gao, Narteau, Rozier, Courrech du Pont, 2015; Zhang et al., 2012). In practice, we calculate Q_{\perp} and Q_{\parallel} , the normal and parallel-to-crest components of transport for each time step i of the wind data and all directions of elongation $\alpha \in [0, 2\pi]$. The direction of elongation α_F is the one for which the normal-to-crest components of transport cancel each other out (i.e., $\sum_i Q_{\perp}^i = 0$) and for which $\sum_i Q_{\parallel}^i$ has the largest value noted $\|\langle \bar{Q}_F \rangle\|$. Considering the speed-up effect ($\gamma \neq 0$), this direction of elongation may differ from the resultant transport direction on a flat sand bed (Rozier et al., 2019).

2.3. Satellite and Field Data

Three satellite images are used to analyze reversing dune morphodynamics, two Landsat images from Google Earth (April 18, 2005 and August 30, 2011 with resolutions of 0.5 and 2 m respectively), another from the ZY-3 satellite (February 14, 2017). Multispectral and panchromatic data of the ZY-3 image have been fused to obtain a 2 m resolution. The image from 2005 has the highest resolution and we use it to select 51 control points for coreferencing. After geometric correction, we achieve a precision of 2 pixels between data sources, which is at least one order of magnitude smaller than the measured displacements.

For each image, we measure the width W and length L of individual dunes, but the resolution is not high enough to obtain estimates of dune slopes on both sides of the crest. The migration rate is derived from the positions of the crest and the length of the dune, L_{t_1} and L_{t_2} , at two different times t_1 and t_2 . By connecting each end of the dune at these two different times, we define the area S_T covered by the migration of the dune during the corresponding time interval. Then, the average migration rate of the reversing dune is computed as the ratio between the characteristic distance traveled by the crest, $2S_T/(L_{t_1} + L_{t_2})$, and the time interval $t_2 - t_1$.

Field surveys in November 2017 and September 2018 provided precise measurements of topographic and granulometric data on several dunes in order to quantify the mean grain size and the dune shape, including height and slopes on both sides of the crest (Figure 1f). Grain size distributions of surface sand samples collected on dunes were determined by a laser particle size analyzer (BT-9300S). In addition, ground-penetrating radar (GPR) profiles perpendicular to the dune ridges were collected using a pulse EKKO PRO system with 500 MHz antennas, a step size of 0.02 m and antenna separation of 0.1 m. Topographic corrections from GPS-RTK measurements have been applied to the GPR data.

3. Reversing Dune Morphodynamics

Here, we present results from different sets of data to establish and quantify the paradox between the eastward migration of the reversing dunes and the resultant westward transport on a flat sand bed.

3.1. Grain Size Distributions and Aerodynamic Roughness

Figure 2a shows the grain size distributions of surface sand on reversing dunes. Both the lee and stoss sides are composed of quartz grains with a diameter d ranging from 150 to 210 μm , in agreement with aeolian sediments in the Taklamakan (Jiang & Yang, 2019). As in most sand seas of the Tarim Basin, a small proportion of coarser particles composed of rounded natural grains of basaltic andesite can accumulate on the flanks of the larger dunes, giving them that darker appearance easily recognizable in the satellite images. These larger grains with a mean grain size close to 500 μm can form mega ripples on the leeward side and at the crest of the dunes (Figure 2c). They have no measurable impact on dune dynamics and all reversing dunes have west-facing slip faces composed of fine grains (Figure 2b). The aerodynamic roughness $z_s = 10^{-3}$ m is determined from the Owen (1964) formula, $C\langle u_* \rangle^2 / (2g)$, where the constant C is taken equal to 0.25 to account for its higher value on dunes with superimposed ripples during periods with saltation (Field & Pelletier, 2018; Sherman & Farrell, 2008). The same value is used for the ERA5 and the local wind tower data.

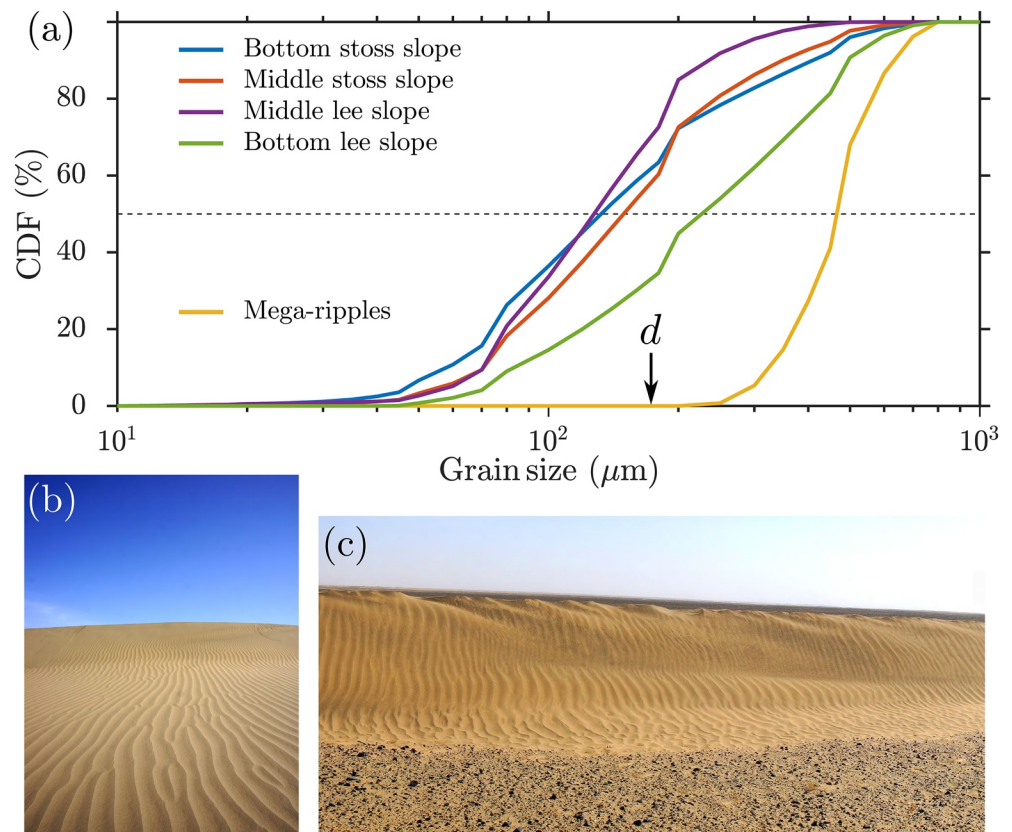


Figure 2. Grain size distributions of surface sand on dunes. (a) Grain size distributions on the lee and stoss sides of dunes. (b) Avalanche face of a dune. (c) Mega ripples at the crest of a dune.

3.2. Characterization of Wind Regime and Sediment Transport

Figure 3a shows the wind and sand flux roses for the local wind tower and ERA5 reanalysis data. For the direct comparison with sand flux roses, wind roses indicate the direction toward which the wind blows, and not the direction from which it comes. Not surprisingly, our local measurements are more dispersed given the higher sampling rate and the turbulent nature of the air flow. Nevertheless, the angular distributions of the wind and the sand flux are consistent for the two sets of data, highlighting the stability of the annual wind cycle measured in the field over the last 30 years. Although the wind and sand flux roses both display bimodal distributions with a prevailing direction to the west-southwest, the secondary peak is not observed in the same range of direction. It is to the north for the wind and to the east-northeast for the sand flux. This is a direct consequence of the nonlinear transport law (Equation 6) and the difference in wind speed distribution between these two specific ranges of wind directions.

In order to elucidate the origin of such a discrepancy, Figure 3b shows variations of wind shear velocity and direction with respect to time over 2 weeks. It illustrates once again the agreement between the two sets of wind data. Both reveal the presence of a regular daily cycle and the random occurrence of strong winds. They are associated with storm events that can last a couple of days. During these extreme events, sediment transport is continuous ($u_* > u_{*c}$) to the east-northeast, a direction of transport never experienced in days without storms. The regular daily cycle is characterized by diurnal sand-transporting winds and weaker winds at night. These nocturnal winds are to the north, while the stronger winds of the day are systematically to the west-southwest. They are caused by large-scale pressure gradient resulting from heating contrasts between the Taklamakan Desert and the surrounding areas. Then, as the wind gets stronger and weaker, it is always driven by the same reorientation mechanisms (Figure 3c). The combined effect of the daily cycle and storms eventually explains the difference between the wind and sand flux roses (Figure 3a).

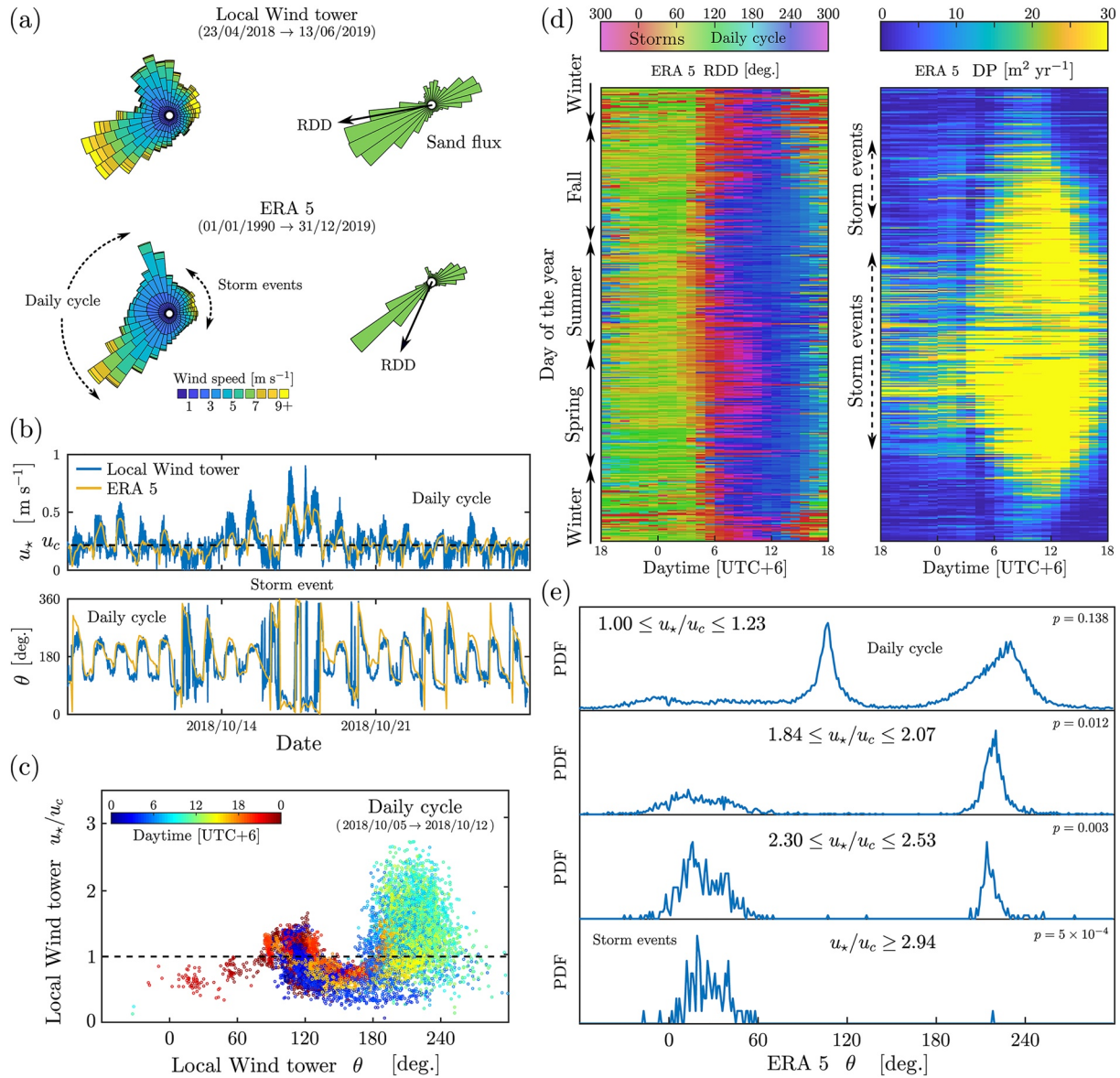


Figure 3. Wind regime in the reversing dune field. (a) Wind and sand flux roses from 30 years ERA5 reanalysis and 14 months local wind tower data. To easily compare wind and sand flux roses, each slice of the wind roses represents wind in that direction. Arrows show the predicted resultant transport direction (Table 1). (b) Wind shear velocity (top) and direction (bottom) for three weeks in October 2018. All directions are measured anticlockwise from the east. A storm hits the dune field on October 17 and 18. The dashed line indicates the threshold wind shear velocity. (c) Wind speed ratio with respect to wind direction for 3 days without storm using the local wind tower. Colors show the time of the day. (d) Orientation (left) and magnitude (right) of the sand flux according to the day of the year and the time of day based on 30 years ERA5 data. (e) Distribution of wind direction according to different ranges of wind speed ratio. The p -value gives the proportion of time the wind is blowing in this speed range. Note that the prevailing wind comes from the east (diurnal phase of the daily cycle). Winds from the south are associated with weak transport (night phase of the daily cycle). Westerly winds are rare but associated with extreme transport events (i.e., storms).

The longer duration of the ERA5 reanalysis data is used in Figure 3d to investigate the annual cycle through seasonal changes in the intensity of the daily cycle and in the frequency of storms. In winter, the study area is influenced by the Siberian high pressure system. The daily cycle is preserved in term of orientation but weakens considerably in term of wind speed. There are almost no transporting winds. For the rest of the year, diurnal winds are predicted to generate significant transport to the west-southwest. As storms happen at all hours of the day, their increasing frequency can be linked to higher rates of transport to the east at night or in the morning. As shown in Figure 3d, this happens mostly in the spring and fall due to the intensification of thermal depressions over Central Asia.

The analysis of the distribution of wind direction for different ranges of wind speed also provides a quantitative description of the relative contribution of the various components of the wind regime on sediment transport (Figure 3e). For speed just above the threshold shear velocity, winds are essentially to the north and to the west-southwest according to the daily cycle. For intermediate shear velocity, the distribution of wind direction is also bimodal but with opposite winds to the east-northeast and the west-southwest. For high shear velocity, the distribution becomes unimodal again but centered around the east-northeast direction of the storm winds. However, the frequency of storms is not high enough to compensate for the daily transport of sand westward (see p -values in Figure 3e).

Finally, both sets of wind data indicate that the diurnal winds of the regular daily cycle govern sediment transport on the alluvial fan of the Molcha river, so that the resultant sand flux is oriented to the west. Such a prediction satisfies the large-scale sand flow path at this southern edge of the Taklamakan Desert (Figure 1a). Meanwhile, the sand flux roses always exhibit two opposite transport directions that together contribute to the development of reversing dunes.

3.3. Dune Orientation and Length Distributions

Multiple dune shapes and various dune orientations are observed on the coarse grain deposits of the alluvial fan. In this zone of low sand availability submitted to frequent wind reversals (Section 3.2), they can all be recognized as reversing dunes. In the vast majority of cases, the crest alignments can be directly related to the underlying dune mechanism considering the two modes of dune orientation (Section 2.2.3). As a consequence, the distribution of dune orientation ranges between the two predicted dune orientations, with a dispersion which is representative of the angular divergence between α_1 and α_p (Table 1 and Figure 4a). Where the dunes develop from patches of sand a few meters thick, they form a periodic pattern oriented in a direction perpendicular to the two main transport directions (Figure 4b). This dune alignment is systematically close to the predicted orientation α_1 of dunes in the bed instability mode. Isolated linear dunes that can reach several hundred meters in length are also distributed throughout the entire area. They all have a north-south alignment close to the predicted orientation α_p of dunes in the elongating mode (Figure 4c). As described by Gadal et al. (2020), the coexistence of the two modes of dune orientation is obvious where long linear dunes elongate southward from the regular dune patterns that develop on the sand patches.

All the reversing dunes are between 0.5 and 2.5 m high regardless of their length, orientation or growth mechanism (Figures 4e and 4f). Dunes of such a small height have a similar turnover time and the relationship between their orientation and length gives more information on the different dynamical aspects of their formation (Figure 4g). As the two main transport directions are almost perpendicular to the dune orientation, the resultant flux along the dune crest is small. Elongation by deposition of the sediment transported along the crest is then inhibited by the permanent sand losses at the dune tips (Rozier et al., 2019). Instead, it is mainly governed by dune-dune interactions and a collision-ejection mechanism that connects their nonoverlapping parts of two dunes perpendicularly to the direction of migration (Gao, Narteau, & Rozier, 2015). In all cases, the upstream end of the elongating dune is mobile and aligned with the bed instability mode. As these dunes get longer, mainly by collisions, they also continuously reorient themselves from α_1 to α_p , the only orientation that prevents the dunes from breaking up as they migrate (Nakao-Kusune et al., 2020). As observed in the field and from satellite images, α_p is therefore an asymptotic orientation for the longest dunes (Figure 4g). Nevertheless, they are still unstable because of wind fluctuations, defects, collisions, and the natural tendency of linear dunes to destabilize as they migrate (Parteli et al., 2011). These breakups are frequent in the reversing dune field, and elongating dunes may rapidly transform in a train of smaller barchan dunes with the orientation of the bed instability mode (Figure 4g). The simultaneous expression of these dune growth mechanisms, dune-dune interactions and breakups explain the diversity of shape, length, and orientation of the population of reversing dunes.

3.4. Dune Migration From Satellite Observations

Visual examination of a temporal sequence of satellite images is enough to conclude that dunes are migrating eastwards. Using the tracks of cars that bypassed or crossed the dunes, the different examples shown in Figure 5 indicate that this is always the case, whatever the geometry of dune interactions or the orientation of the dunes. Over one decade, the distance traveled by the dunes is of the order of a 100 m (Figure 5). In addition, the

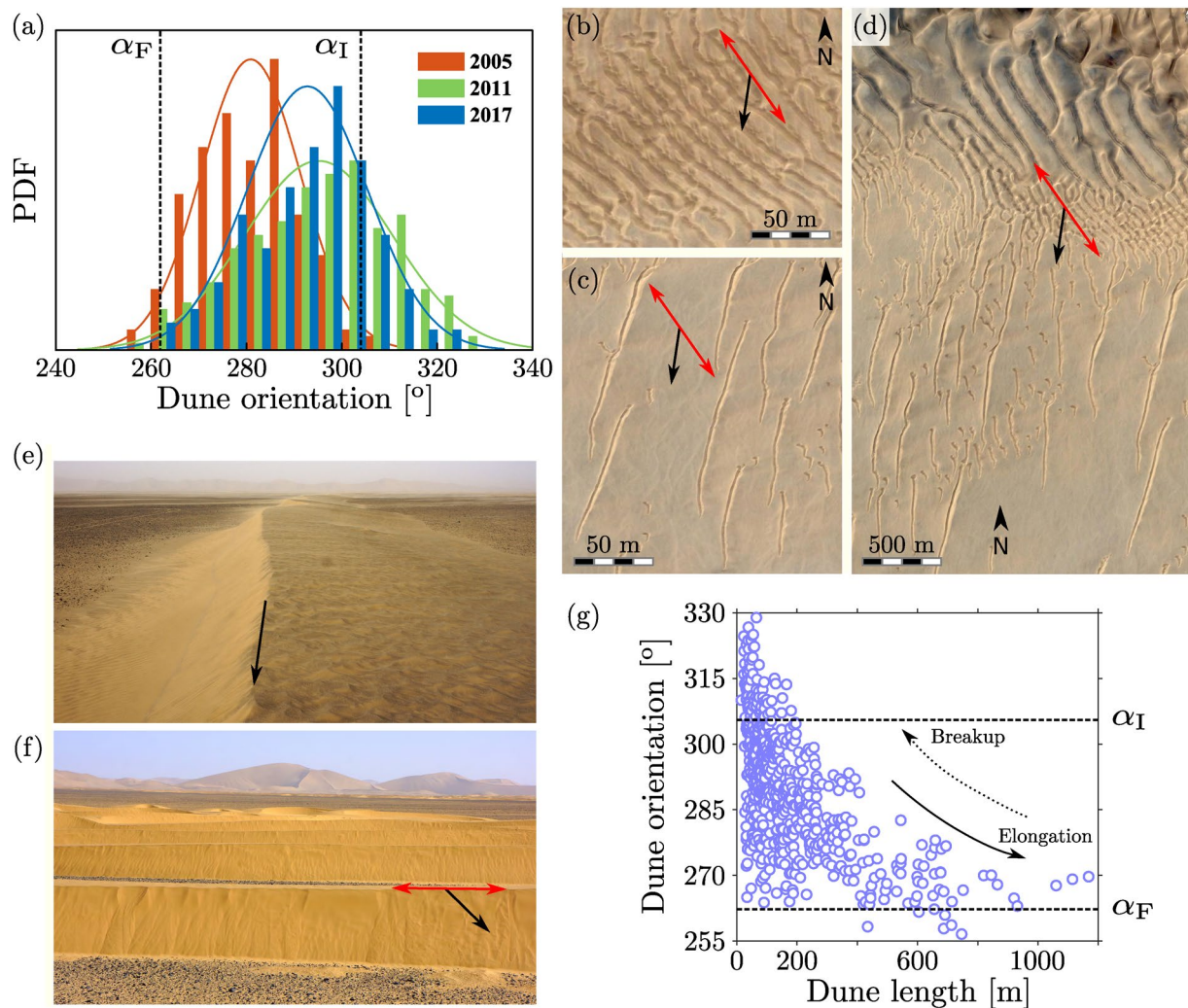


Figure 4. Coexistence of two dune growth mechanisms with different orientations in the reversing dune field. (a) Distribution of dune orientation at three different times. Dashed lines show the dune orientations predicted from the wind data for the bed instability and the elongating modes (Table 1). In (b–f), these predicted dune orientations α_I and α_F are shown by double red arrows and black arrows, respectively. (b) Periodic dune pattern in the bed instability mode. (c) Isolated elongating dunes. (d) Dunes elongating from a periodic dune pattern. (e) Longitudinal view of an elongating dune. (f) Transverse view of periodic dunes in the bed instability mode. Giant dunes in the background are to the east. (g) Relationship between dune orientation and dune length. Elongating dunes grow from deposition at the tip of periodic dunes in the bed instability mode (Gadal et al., 2020) and mainly from dune-dune interactions (i.e., collisions). They eventually break up and disappear as they migrate.

persistence of hydrological patterns, such as braided channels and bars, reveals that dune dynamics are much more active than the alluvial fan dynamics, at least in the last 20 years during which anthropogenic impact on the Molcha River has increased considerably (water control structures and dams at the outlet of the watershed).

Figures 6a and 6b show the evolution of two populations of reversing dunes from 2005 to 2017. These examples demonstrate that reversing dunes migrate eastward with a remarkable regularity, keeping the same size, shape and sinuosity in many cases. However, collisions, defect migrations or breakups can also be observed. The smallest and most isolated dunes have the highest probability of disappearing. Averaged over dunes identified on all satellite images, the mean migration rate for this 12-year period is of 8.6 m year⁻¹, with a higher rate of 11.4 m year⁻¹ between 2005 and 2011 and a smaller one of 6.6 m year⁻¹ between 2011 and 2017 (Figure 6c). For the same time periods, the distribution of the direction of dune migration has a clear peak to the east, with a standard deviation of less than 15° (Figure 6d).

The dune aspect ratio H/W measured in the field has a mean value of 0.0728, which corresponds to widths of 14 and 27.5 m for dune heights of 1 and 2 m, respectively. Using this aspect ratio and the dune widths measured on

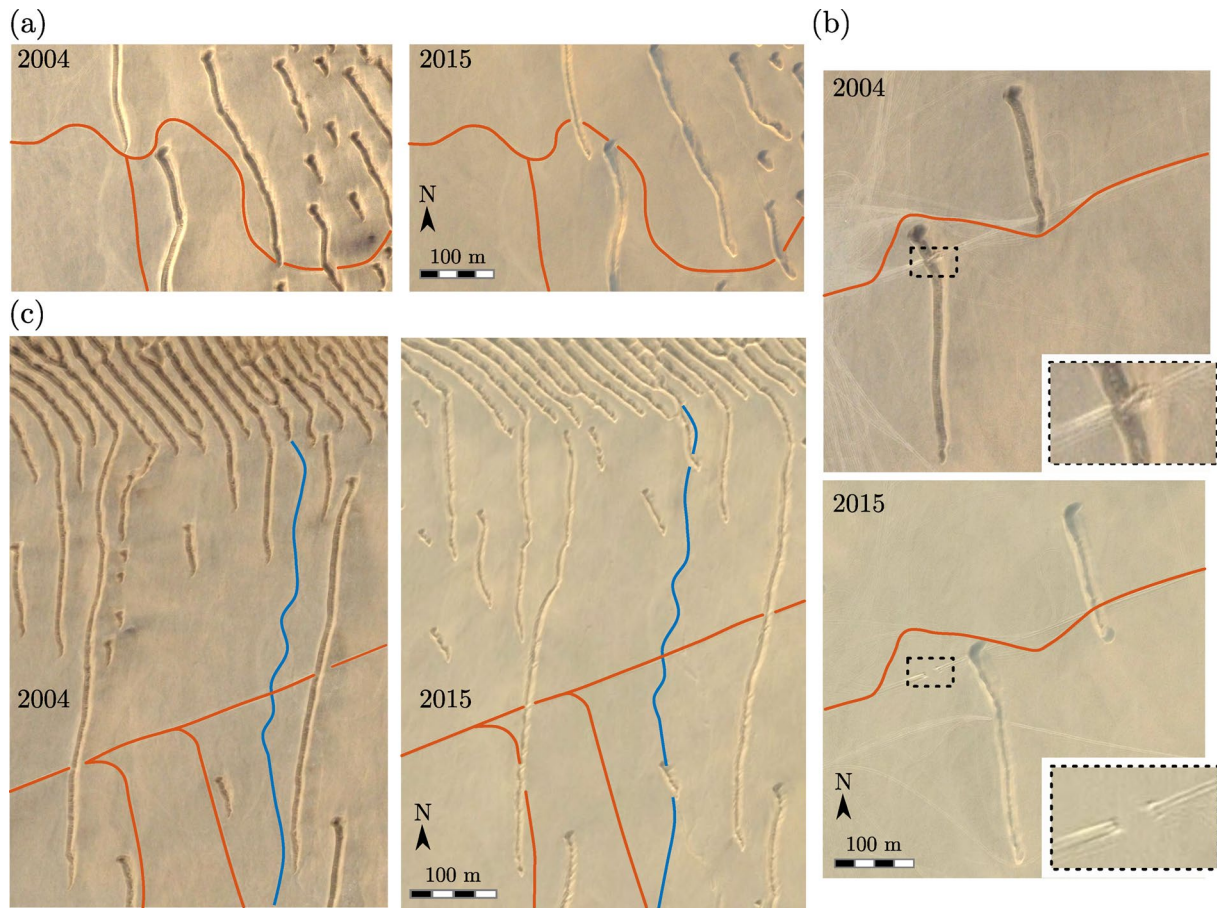


Figure 5. Examples of eastward migration of reversing dunes. (a) Two dunes offset to the right (84.45°E, 37.63°N). (b) Two dunes offset to the left (84.47°E, 37.62°N). Migration of dunes combined with the preservation of car tracks (red curves) illustrate the chronology of our satellite images. Insets show that cars cutting over active dunes leave discontinuous tracks on the gravel bed of the alluvial fan after dune migration. (c) Dunes in the bed instability and the elongating modes (84.49°E, 37.63°N). A stream channel is highlighted in blue.

satellite images, Figure 6e shows the dune migration rate c with respect to dune height. The observed dispersion of the data is easily explained by the narrow range of dune widths and the precision of ± 1 m of our measurements (i.e., ± 2 pixels). Fitting to the data the relation $c = \|\bar{Q}_{\text{crest}}\| / H$, a dune of 1 m high is predicted to migrate eastward at a rate of 14.6 m year⁻¹. This corresponds to an eastward sand flux $\|\bar{Q}_{\text{crest}}\| = 14.6 \text{ m}^2 \text{ year}^{-1}$ at the crest of the dunes. This sand flux is of the same order of magnitude as the predicted sand flux $\langle \bar{Q}_1 \rangle$ at the crest of dune in the bed instability mode (Table 1), but is opposite in term of orientation. There is therefore a rather considerable difference of nearly 30 m² year⁻¹ between the sand flux predicted from the wind data and those derived from the migration of reversing dunes.

3.5. Dune Migration From Ground-Penetrating Radar Surveys

Figure 7 shows the 500 MHz GPR profile as well as an interpretation of the dipping strata and bounding surfaces within a transverse section of a 2.5 m high reversing dune. Interestingly, the base of the dune can be easily identified thanks to the high-amplitude reflections at the surface of the coarse grain deposits of the alluvial fan.

The internal structure of the dune can be decomposed into two major radar facies, characterized by inclined reflection patterns with different orientations. At the bottom of the dune, three-quarters of the dune section is dominated by sets of cross-stratification dipping to the east. These high-angle inclined reflections provide evidence for the dune migration from the west to the east, which is in agreement with the migration direction derived from satellite images. At the top of the dune, east-dipping strata are truncated by a low-angle bounding surface. This bounding surface and all the lower-angle inclined reflections above dip to the west. These stratifications are

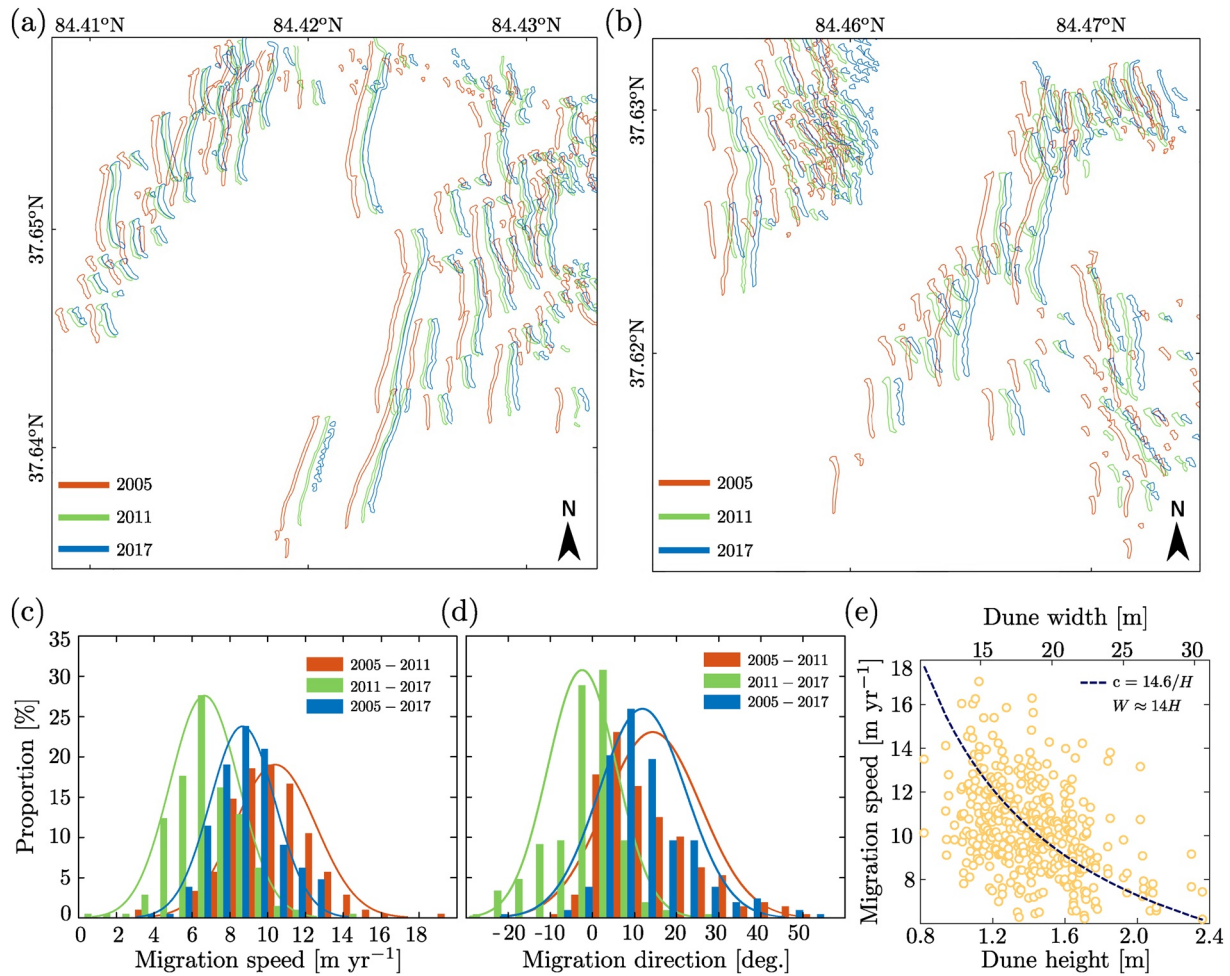


Figure 6. Statistics on migration of reversing dunes. (a–b) Estimation of the position of dunes at three different times using satellite images. Note that the more the dune is isolated, the more it breaks up and disappears. (c–d) Distributions of dune migration speed and direction over three different time periods. Solid lines are the best fits to the data using normal distributions. (e) Dune migration rate with respect to dune height. The dashed line is the best fit of a $\|\bar{Q}_{\text{crest}}\|/H$ hyperbolic function to the data.

associated with a wind reversal followed by a prevailing easterly wind, which was observed in the field during the measurements. All the GPR profiles acquired on transverse sections of neighboring reversing dunes show similar sedimentary structures. Thus, shallow subsurface stratigraphies confirm that dunes are systematically reshaped by two alternate winds blowing from both sides of the crest with high angle of incidence. More importantly, they also demonstrate that, despite frequent crest reversals, the overall migration of the dune is to the east.

3.6. Sensitivity Tests on the Dune Migration Paradox

Considering sand fluxes derived from both sets of wind data together with field and satellite observations, there is therefore an apparent paradox between the eastward migration of the reversing dunes and the westward resultant transport on a flat bed. We test the robustness of this dune migration paradox with respect to climatic conditions that might affect sand transport, the transport law and the uncertainties of different parameters used to estimate the threshold shear velocity. These tests are based on a quantitative estimation of the transport deficit at the crest by computing the difference between the sand flux deduced from the observed dune migration, $\|\bar{Q}_{\text{crest}}\|$, and the eastward component of the sand flux predicted from wind data, $\|\langle \bar{Q}_1 \rangle\| \cos(\theta_{Q_1})$.

As shown in Figure 8a, the deficit in transport is close to $34 \text{ m}^2 \text{ yr}^{-1}$ for grain size d of $180 \mu\text{m}$ and an aerodynamic roughness z_s of 10^{-3} m (Table 1), and remains larger than $10 \text{ m}^2 \text{ yr}^{-1}$ in the limit of coarse sand and low

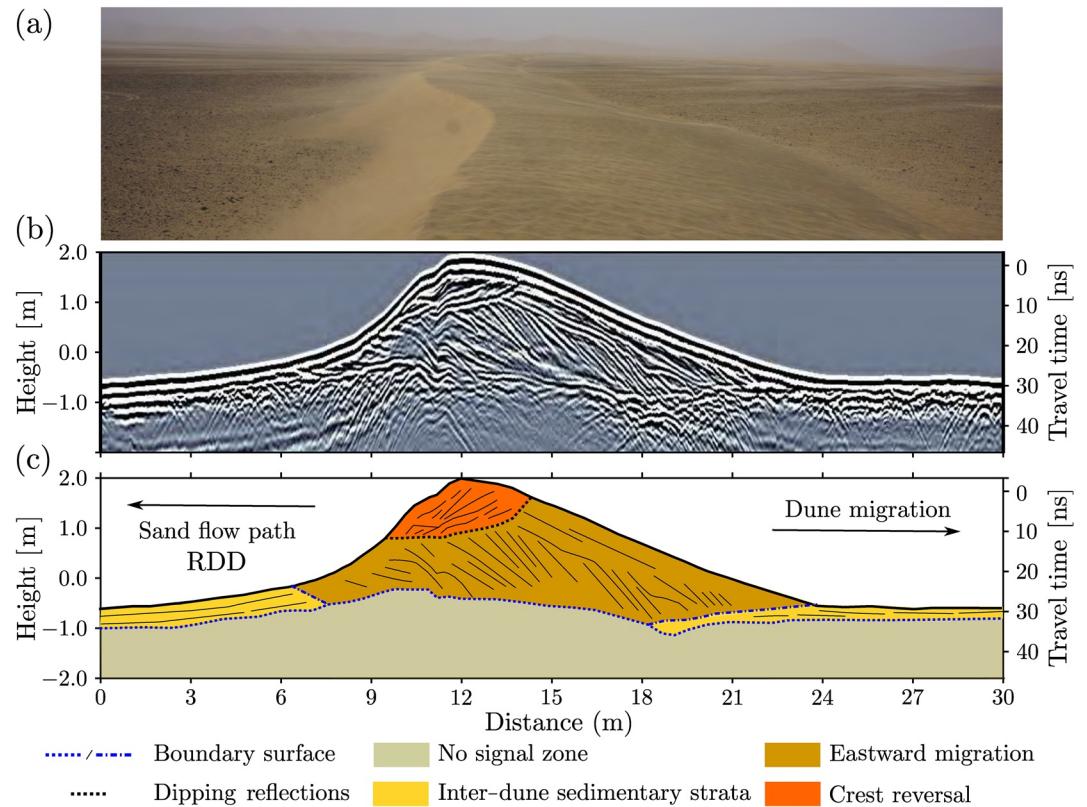


Figure 7. Bounding surfaces in a reversing dune. (a) Longitudinal view of the elongating dune just before the radar survey. (b) Ground-penetrating radar (GPR) profile of the cross-section of the reversing dune. (c) Interpretation of the bounding surface within the dune. West-facing reflections in the crest reversal section at the top of the dune agree with the current wind regime and the diurnal easterly wind of the daily cycle, east-facing reflections of the internal section are consistent with the eastward migration of the dune.

aerodynamic roughness. Under these conditions, the paradox of dune migration is avoided in terms of orientation, the dune migration rate is three times smaller than that observed and daily winds should not generate transport. In addition, dunes with east-facing slip face should be mainly composed of coarse grains and show sign of elongation toward the north-northeast. However, this is not the case. Instead, dunes are mainly composed of fine grains, there are many evidence for transport during the daily winds (Figures 1c, 1d and 2b), not only on dunes but also in the interdune areas (Figures 8b and 8c).

Recent laboratory experiments and numerical simulations highlight a transition from saltation to collisional regime above a critical transport rate, which can typically be reached during storm winds in our site (Pächt & Durán, 2020; Ralaiarisoa et al., 2020). Then, a quadratic relationship such as Equation 6 underestimates sand transport compared to the quartic relation recently proposed by Pähtz and Durán (2020), or overestimates it by not taking into account intermittent transport due to turbulent fluctuations (Comola et al., 2019; Pähtz et al., 2020). Using the theoretical model proposed by Comola et al. (2019), we find no significant change in the sensitivity analysis presented in Figure 8a. However, a quartic law significantly increases the transport deficit, such that the dune migration paradox is reinforced in the entire parameter space.

Finally, frost, precipitation, and differences in drying rate between strong winter and light summer winds can also modify transport, as shown on active transgressive dune fields by Hesp and Thom (1990). Nevertheless, using the ERA5-Land climate reanalysis data, we find that the potential evaporation is always at least one order of magnitude higher than precipitation (including snowfall, etc.) and that the local aridity index has a mean value of 0.02 that corresponds to hyper-arid environments (Spinoni et al., 2015). Precipitation time steps represent only 2% of the time, less than 5% of the total predicted transport and are only associated with eastward sand fluxes. Surface layer temperatures are negative in winter, but the water content is less than 3% and throughout this period

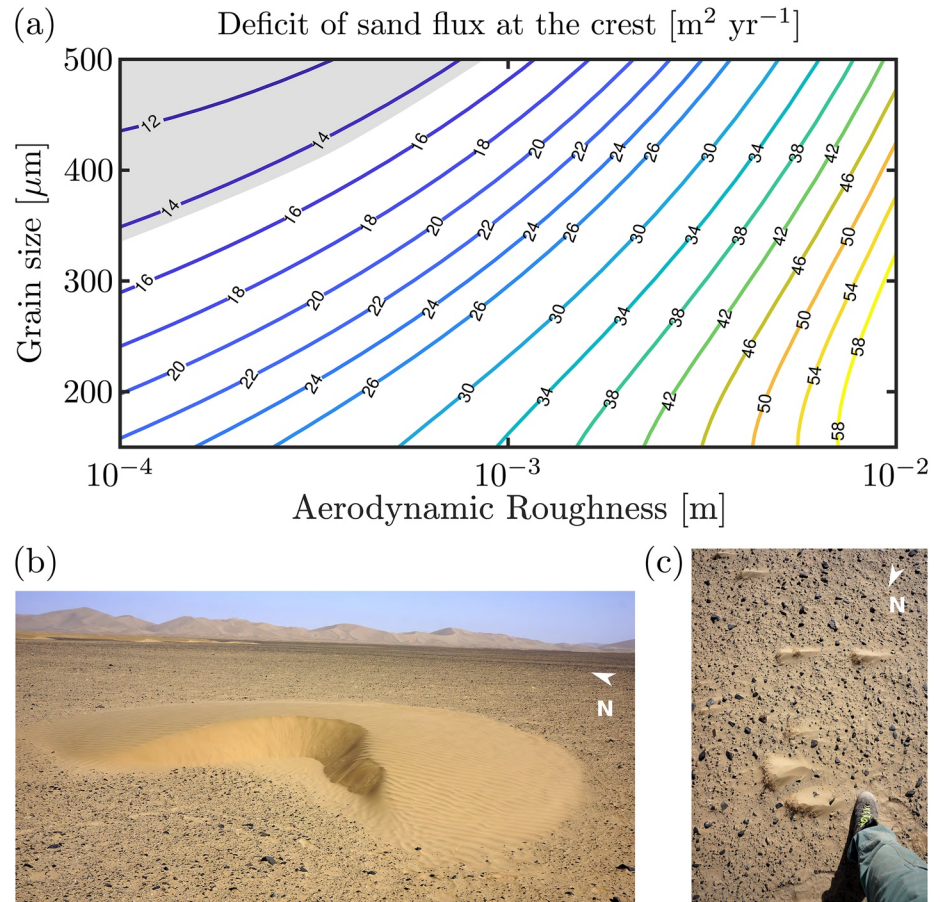


Figure 8. The dune migration paradox. (a) Sensitivity analysis of dune migration to grain size d and aerodynamic roughness z_s . Contour lines show the difference $\|\bar{Q}_{\text{crest}}\| - \|\langle \bar{Q}_1 \rangle\| \cos(\theta_{\bar{Q}_1})$ between the sand flux at the crest estimated from dune migration (Figure 6) and the eastward component of the sand flux predicted from the local wind data. The shaded area shows values for which the predicted resultant sand flux on a flat sand bed and the dune migration are to the east (i.e., no dune migration paradox). Nevertheless, under such conditions, the dune migration rate is predicted to be at least three times slower than the observed ones and the observed dunes should be entirely composed of coarse grains ($d > 350 \mu\text{m}$) with east-facing slip faces. (b) Crescentic dunes and (c) sand deposits after small obstacles showing transport of fine sand ($d < 200 \mu\text{m}$) to the west associated with the primary wind of the daily cycle.

the wind is extremely weak and again associated with eastward transport (Figure 3d). Hence, if local climatic conditions are responsible for a reduction in transport via cohesion, they would increase the transport deficit and thus reinforce the dune migration paradox.

4. Modeling Sand Fluxes and Migration of Reversing Dunes

Once the dune migration paradox is established, there is a need to reevaluate our estimates of the sand flux at the crest of dunes, which fully determines the migration speed and direction of these dunes. First, we use a 2D version of a cellular automaton dune model (Narteau et al., 2009; Rozier & Narteau, 2014) to obtain quantitative evidences on the dynamical processes that are not involved in our current procedure of sand flux estimation at the crest of dunes (Section 4.1). Then, changes in dune shape after wind reversal are incorporated into our procedure to test if the apparent dune migration paradox can be resolved (Section 4.2).

4.1. Flux at the Crest of Reversing Dunes in a Cellular Automaton Model

The cellular automaton dune model implements a complete feedback mechanism between flow and bed-form dynamics, so that the shear velocity and sand flux adapt to any changes in dune shape (Narteau et al., 2009;

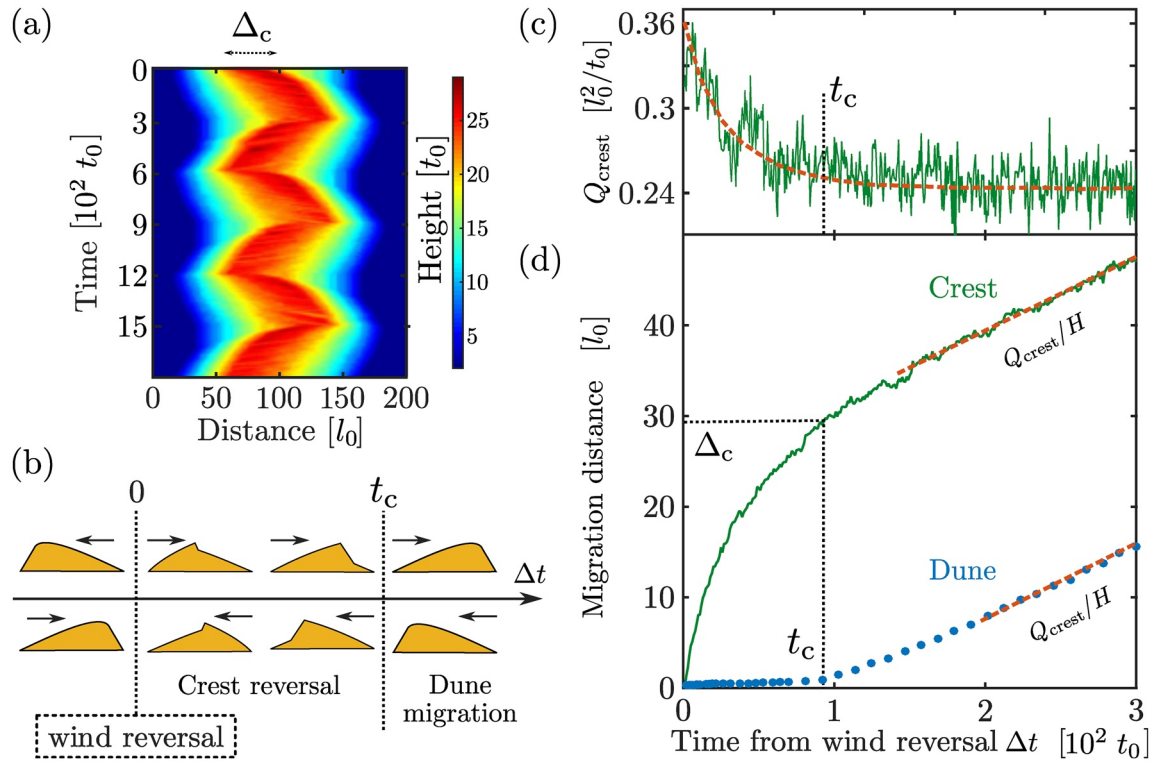


Figure 9. Dynamics of reversing dunes and sand fluxes in a 2D cellular automaton dune model using two alternating winds of opposite direction and equal duration $\Delta T = 300 t_0$. (a) Space-time diagram of the elevation profile of the reversing dune over three wind cycles when the stationary oscillating regime is reached. Δ_c is the crest reversal distance. (b) Sketches illustrating changes in dune shape with respect to the time Δt from the last wind reversal. Arrows show wind directions. (c) Sand flux at the crest with respect to the time from the last wind reversal. (d) Crest (green) and dune (blue) migration distances with respect to the time from the last wind reversal. After the characteristic time t_c , the crest traveled a distance Δ_c , the slip face has fully reversed and the dune shape has reached its steady state. The sand flux at the crest is constant and the migration rates of the dune and the crest are equal (dashed lines).

Rozier & Narteau, 2014). As it was the case for the formation and migration of superimposed bedforms under unidirectional wind regimes (Zhang et al., 2010), this model can, therefore, provide detailed information about the transient behaviors associated with wind and crest reversals. In a 2D version of the model, we consider two alternate winds from opposite directions but of equal strength and duration. Expressed in the time scale t_0 of the model (Narteau et al., 2009; Zhang et al., 2014), individual winds blow for $\Delta T = 300 t_0$ and the entire wind cycle lasts $2\Delta T$. The initial condition is a sand bar of $25 l_0$ high and $50 l_0$ wide in the center of a wide and flat nonerrodible domain, where l_0 is the elementary length scale of the cellular space.

After a few wind cycles, a reversing dune reaches a stationary regime characterized by periodic oscillations of the positions of the crest and of the upwind and downwind boundaries of the dune (Figure 9a). The shape and dynamics of the dune are symmetrical with respect to the two winds, so that the dune is not mobile when averaged over the entire wind cycle (Rozier et al., 2019; Zhang et al., 2012). The transport associated with each wind is large enough to remobilize the entire dune and, after a time interval t_c following each wind reversal, the dune reaches its steady shape with a slip face extending downwind over its whole height (Figure 9b). Hence, after each wind reversal, the wind always hits a slip face and starts to flatten the new stoss face. Then, t_c is the time interval required for the new slip face to develop on the other side of the dune. It occurs when the crest has migrated downwind over the characteristic distance Δ_c (Rozier et al., 2019). For each period of constant wind, dune dynamics is thus divided into two successive phases, a crest reversal phase followed by a uniform migration when the steady shape is reached.

Most important for our present purposes, the sand flux at the dune crest varies during these different phases. Due to the speed-up effect, the sand flux is high just after wind reversals and relaxes to a constant value over the characteristic time t_c (Figure 9c). During this time interval, the crest is moving rapidly, the stoss slope flattens and the upwind and downwind boundaries of the dune move only over short distances. Later, both the crest and the

dune are migrating at the same speed downwind (Figure 9d). Wind reversals are therefore associated with abrupt changes in the apparent dune aspect ratio and nonlinear variations in the sand flux at the crest. These transient changes in dune shape are not taken into account in our sand flux estimation procedure (Section 2). However, under specific wind regimes, this nonlinear response of the sand flux to sudden changes in wind direction is likely to strongly affect dune migration.

4.2. Modeling the Impact of Crest Reversal on Dunes Migration

To account for crest reversals and transient changes in dune shape, it is necessary to develop an iterative procedure that successively updates the apparent aspect ratio of the dune, with respect to wind strength and direction. We develop here such a procedure in 2D to investigate the impact of opposite winds with different strengths and durations on dune migration.

Let us consider a triangular dune of constant width W and height H (Figure 10a). The only variable to characterize dune shape is the position x_c of the crest with respect to the position of the dune. By definition, $x_c = 0$ when the dune has a symmetrical shape. The angle of repose Θ of the granular material together with the dune width and height determines the maximum crest reversal distance $\Delta_c = W - 2H/\tan(\Theta)$. Then $-\Delta_c/2 \leq x_c \leq \Delta_c/2$. When $x_c = \pm\Delta_c/2$, the dune has a slip face on either of these two sides, and until the next wind reversal, it migrates keeping its steady asymmetric shape. Otherwise, the crest is migrating and the dune is changing shape.

Implementing these rules, the amount of sediment transported at the crest between t and $t + \delta t$ is

$$S = \|\bar{Q}_{\text{crest}}\| \delta t = \|\bar{Q}_{\text{flat}}\| \left(1 + 2\beta \frac{H}{W/2 - x_c}\right) \delta t, \quad (12)$$

Since $x_c \neq \pm\Delta_c/2$, the crest migrates a distance

$$\delta x = \pm \frac{2SW}{HW - 2S}, \quad (13)$$

where the sign corresponds to the two possible wind directions. In the limit of $\delta t \rightarrow 0$, Equations 12 and 13 can be used to successively compute the position of the crest as well as the corresponding sand flux. Then, in order to estimate the cumulative transport at the crest, the sequence of winds is critical because the sand flux depends on the current shape of the dune.

This iterative procedure is implemented on a 2 m high and 28 m wide dune using the ERA5 wind data. Figure 10b shows the cumulative sand flux on a flat sand bed and at the dune crest. We assume that this dune has the alignment of bed forms in the bed instability mode and we only consider the projections of the sand flux vectors \bar{Q}_{flat} and \bar{Q}_{crest} onto the direction perpendicular to α_1 . We also take $\beta = 0.4(W - \Delta_c)/H$ to keep the same intensity of the speed-up effect as in our previous analysis when $x_c = \pm\Delta_c/2$ (i.e., $\gamma = 1.6$). In agreement with field observations, the model predicts a resultant sand flux at the crest which is against the direction of the resultant transport direction on a flat sand bed. While the westward trend of the cumulative transport on a flat sand bed is regular and smooth, the eastward trend of the cumulative transport at the crest is more discontinuous with sharp increases in spring. The periodic impact of storm winds is evident despite the variability in storm intensity from year to year. In agreement with field observations and despite the eastward migration of the dune induced by the resultant sand transport at the crest, the west-facing face of the dune in the model is most of the time steeper than its east-facing one (Figure 10c).

The apparent dune migration paradox seems to be resolved, but the natural variability of the wind and our lack of regular dune elevation profile in the field prevent at this stage a more detailed quantitative analysis. Hence, we test the model against a synthetic wind regime representative of the current conditions in the reversing dune field. The daily cycle consists of two opposite winds of equal strength ($u_* / u_c = 1.06$) but of different durations: 17 and 7 h for the primary and secondary winds, respectively. After 150 days of this regular daily cycle, a storm event ($u_* / u_c = 3.31$) with the orientation of the secondary wind hits the dune for 96 h. The wind regime consists of the periodic succession of these two phases.

Using this synthetic wind cycle in our new iterative procedure on 2 m high and 28 m wide dune, Figure 10d shows once again that the cumulative sand flux on a flat sand bed and at the crest are opposed to one another.

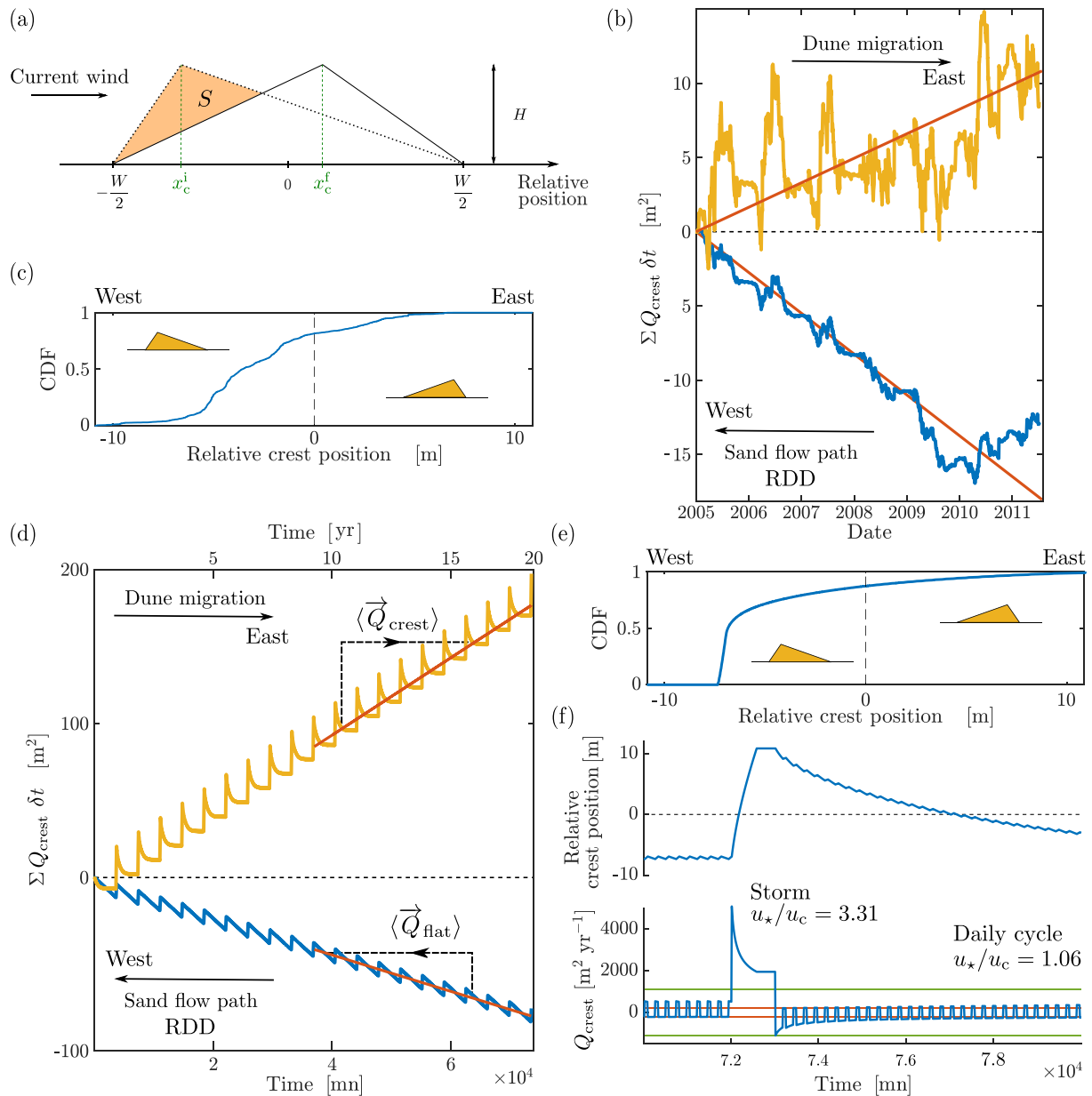


Figure 10. Modeling the impact of crest reversal on dune migration. (a) A model for the evolution of dune shape after wind reversal. Dune width W and height H are constant. $x_c^{(i,f)}$ are the relative position of the crest before and after a period of constant wind (Equations 12 and 13). (b) Cumulative sand flux on a flat sand bed (blue) and at the crest of a 2 m high and 28 m wide dune (yellow) using ERA5 wind data. Red lines are linear fits to the data. (c) Cumulative distribution function of the position of the crest relative to dune width. (d) Cumulative sand flux on a flat sand bed and at the crest of a 2 m high and 28 m wide dune using a wind regime representative of the study area (see text). The west direction is associated with the primary wind of the daily cycle. Storms are assumed to blow to the east. (e) Cumulative distribution function of the relative position of the crest using the same wind regime. (f) Relative position of the crest and sand flux at the crest before, during and after a storm event. Red and green lines show the sand flux at the crest when the daily cycle wind hits the stoss and slip slopes of a dune in steady state, respectively.

The resultant sand transport on the flat sand bed is set by the direction of the primary wind of the daily cycle ($\|\bar{Q}_{\text{flat}}\| = 10.3 \text{ m}^2 \text{ yr}^{-1}$), while the resultant sand flux at the crest ($\|\bar{Q}_{\text{crest}}\| = 21.8 \text{ m}^2 \text{ yr}^{-1}$) is set according to the orientation of storms winds. These sand fluxes are on the same order of magnitude of the sand fluxes derived from the two sets of wind data (Table 1) and from the dune migration rate in the field. As for the ERA5 wind data (Figure 10b), the cumulative sand transport on a flat sand bed is smoother than the one at the crest of dunes, and we clearly distinguish the occurrence of storms. The west-facing face of the dune in the model is also most of the time steeper than its east-facing one, so that Figures 10c and 10e exhibit similar distributions.

In Figure 10f, we investigate the nonlinear feedback between dune shape and sand flux at the crest, which is responsible for the apparent dune migration paradox. When a storm occurs, the dune is always in its steady shape with a slip face generated by the primary wind of the daily cycle. The wind reversal, the increase in wind speed and the speed-up effect combine to produce a sharp increase in sand flux. Then, as the crest reversal occurs, the apparent aspect ratio of the dune decreases and the sand flux relaxes to a stationary value, which is attained when the dune has reached its new steady shape. At the end of the storm, the primary wind of the daily cycle hits also a steep slope, but at a lower speed and for a shorter time. The asymmetry of transport during the daily cycle is not high enough for a complete crest reversal over one day. As a consequence, it takes many days for the crest to migrate back to its original steady state. While this is happening, the contributions to the resultant transport from the two winds of the daily cycle also vary and tend to be balanced. Indeed, there is a longer time period before the next storm during which the secondary wind of the daily cycle is associated with higher transport rate than the primary wind.

Considering together all these behaviors, we can conclude that the apparent dune migration paradox relies essentially on the asymmetry of the dune when storms occur and during the much longer period in which it is subjected to the daily wind cycle. In the study area, this translates into westerly winds blowing systematically on steeper dune slopes than those encountered by easterly winds.

5. Discussion

The reversing dunes on the alluvial fan of the Molcha River are a striking manifestation of the wide variety of shapes and orientations that dune fields subjected to winds from opposite directions can present. Located in a zone of low sand availability, these spectacular dune features are particularly interesting because of their small sizes and the short time scales that are associated with them. More easily than for the giant dunes, their dynamics can be related to their morphology to investigate key issues in dune physics. Here, we have taken advantage of this to show that the mass balance of windblown sand at the dune crest remains an open area of research, even without calling for turbulent structures of the flow. Elementary processes such as the speed-up effect and wind reversals can indeed introduce nonlinearities responsible for important and largely unexplored behaviors. Obviously, the linear dependence of the speed-up on the dune aspect ratio is a simplified representation of the air flow, especially on the steepest dune slopes where recirculations may occur. Nevertheless, even the reworking of a former slip face as a stoss slope is associated with large speed-up at the crest of reversing dune (Neuman et al., 1997). Then, a more precise description of the flow over an evolving dune topography is still needed, but the conditions for the paradox of dune migration will always depend more on wind regimes and dune size than on the detailed expressions of the speed-up.

Considering the linear speed-up effect and the dune aspect ratio experienced by individual winds (Equation 12), the magnitude of the sand flux at the crest can vary by nearly a factor of five depending on whether the wind impacts a gentle slope of 6° or a slip face (i.e., $(1 + 2\beta \tan(\Theta))/(1 + 2\beta \tan(\pi/30)) \approx 5$). These changes are also proportional to the sand flux which increases as the square of wind speed (Equation 6). Then, even without taking into account the transport threshold, variations of more than an order of magnitude can easily occur after wind reversal. These variations can explain the difference in aspect ratio and growth rate between transverse and reversing dunes observed by Gadal et al. (2019) in subaqueous experiments. Averaged over the entire wind cycle, we find here that they can cause reversing dunes to migrate against the sand flow path. Obviously, it requires a specific wind regime. At the southern edge of the Taklamakan Desert, on the flanks of the Tibetan Plateau, it takes the form of an alternation between a regular daily transport and storm events with winds from the opposite direction (Figure 3). Interestingly, it can be noted that opposite flow directions are ubiquitous over subaqueous bedforms in tidal environments or at the head of submarine canyons (Doré et al., 2018; Ernsten et al., 2005; Lo Iacono et al., 2020). Given all possible sources of tidal asymmetry and the fact that extreme events also occur in these environments, the observations made here on aeolian dunes have equivalents in oceanic settings.

While resolving the apparent dune migration paradox, this study illustrates the need for more detailed analysis on the dependence of dune morphodynamics on the sequence of winds. There are many places on Earth and on other planetary bodies where the dune system could strongly depend on the order in which the different winds occur (Bourke, 2010; Charnay et al., 2015; Jackson et al., 2020; Lucas et al., 2014). Taking into account this sequence of winds could further reduce the apparent complexity of dune fields and explain the coexistence of different dune

patterns. However, it will also provide more solutions to the inverse problem of predicting the wind regime from dune shape and orientation (Fernandez-Cascales et al., 2018), which will therefore be more difficult to solve.

A time-based iterative approach is necessary to properly account for the sequence of winds and the nonlinear aspects that govern dune morphodynamics. Numerical models encoding the basic feedback mechanisms between flow and topography seem to be the most appropriate (Narteau et al., 2009; Parteli et al., 2009). Nevertheless, these models often require an excessive amount of computational resources and may encounter numerical diffusion problems when investigating winds of highly variable orientation over large dunes. It would also be possible to consider models in which the transport direction and the threshold shear stress for entrainment are affected by the local dune slope (Gadal et al., 2019; Iversen & Rasmussen, 1994). Given the west-facing slip faces observed in the field, these effects should reduce the transport associated with storm events and reinforce the dune migration paradox. They are therefore not as critical as the speed-up effect, especially when considering the sand flux at the crest.

The simplistic 2D model presented in Section 4.2 is not sufficient to deal all the diversity of dune fields. For instance, it does not consider the exact geometry of crest reversal and cannot deal with superimposed bedforms. However, it is still useful to estimate the potential impact of a given sequence of winds on dune morphodynamics. For example, according to the model, there is only a range of dune heights for which the non-linearities in speed-up generate the apparent dune migration paradox. Then, in agreement with field and satellite observations, the giant dunes surrounding the study area are predicted to migrate along the sand flow path opposite to the migration of the metric high reversing dunes.

The role of extreme events is an active research topic in aeolian research and more generally in landscape dynamics. For example, the impact of storm events is actually widely discussed in coastal areas, where high wind speed combined with energetic wave conditions may cause large-scale erosion of the coastal dunes (Castelle et al., 2015, 2019). It is also well known that infrequent storms hit all the major dune systems on Earth, Mars, and Titan (Leovy, 2001; Rodriguez et al., 2018). We present here the concrete and surprising consequences that seasonal winds can have on dune migration. We find that regular transitions between high frequency low wind episodes and low-frequency storm wind episodes can determine the entire dynamics of the dune system. As the dunes adapt their shape to the current wind conditions, they become increasingly sensitive to perturbations. The continuous evolution of the dunes must therefore be taken into account at the same level as the magnitude and frequency of the perturbations to which they may be subjected. This can become critical in the increasing number of aeolian environments where the resilience of dunes to extreme events needs to be assessed (e.g., transgressive, arid, or extraterrestrial dune fields).

Despite the accuracy of the methods that can now be carried out in dune fields, this study shows that efforts are still needed to successfully predict the shape, the orientation and the dynamics of dunes under natural wind regimes. Taking as an example the crest reversals of small dunes, it seems obvious that this will require finer descriptions of secondary dune patterns and collective behaviors within dune fields.

6. Conclusion

By taking as an example the paradox of the migration of reversing dunes against the sand flow path in a zone of low sediment availability, we quantitatively illustrate the critical impact of the wind speed-up in dune physics. The speed-up effect combined with frequent crest reversals can be responsible for strong and nonlinear variations in transport rate, especially at the dune crest. When integrated over the whole wind cycle, these nonlinearities can exert control over the whole dynamics of a dune field. Such a control of the wind sequence on dune morphodynamics is even more pronounced when extreme events are involved. These results can now be used to explain the diversity of bed forms and their evolution in aeolian (or subaqueous) dune systems on Earth and other planetary bodies where flow reversals are likely to occur.

Data Availability Statement

The authors used ReSCAL software (available at <http://www.ipgp.fr/rescal> with dedicated parameters) for numerical simulations. They use surface wind data from the ECMWF ERA5 Reanalysis. Satellite images in Figures 1, 4 and 5 are courtesy of Google Earth.

Acknowledgments

Xin Gao acknowledges the financial support from the National Natural Science Foundation of China (No. 41971017 and 41861144020), the Strategic Priority Research Program of the Chinese Academy of Sciences (No. XDA20030102), the National Thousand Talents Program (No. Y772091001) and the High-level Talent Cultivation Project from the Xinjiang Institute of Ecology and Geography, Chinese Academy of Sciences (No. E0500201). Clément Narteau acknowledges support from the UnivEarthS LabEx program (No. ANR-10-LABX-0023), the IdEx Université de Paris (No. ANR-18-IDEX-0001), the French National Research Agency (No. ANR-17-CE01-0014/SONO) and the National Science Center of Poland (No. 2016/23/B/ST10/01700).

References

- Andreotti, B., Fourrière, A., Ould-Kaddour, F., Murray, B., & Claudin, P. (2009). Giant aeolian dune size determined by the average depth of the atmospheric boundary layer. *Nature*, *457*, 1120–1123. <https://doi.org/10.1038/nature07787>
- Arens, S. M., Van Kaam-Peters, H. M. E., & Van Boxel, J. H. (1995). Air flow over foredunes and implications for sand transport. *Earth Surface Processes and Landforms*, *20*, 315–332. <https://doi.org/10.1002/esp.3290200403>
- Bourke, M. C. (2010). Barchan dune asymmetry: Observations from Mars and Earth. *Icarus*, *205*, 183–197. <https://doi.org/10.1016/j.icarus.2009.08.023>
- Bristow, C. S., Augustinus, P. C., Wallis, I. C., Jol, H. M., & Rhodes, E. J. (2010). Investigation of the age and migration of reversing dunes in Antarctica using GPR and OSL, with implications for GPR on Mars. *Earth and Planetary Science Letters*, *289*, 30–42. <https://doi.org/10.1016/j.epsl.2009.10.026>
- Britter, R. E., Hunt, J. C. R., & Richards, K. J. (1981). Air flow over a two-dimensional hill: studies of velocity speed-up, roughness effects and turbulence. *Quarterly Journal of the Royal Meteorological Society*, *107*, 91–110. <https://doi.org/10.1002/qj.49710745106>
- Burkinshaw, J., & Rust, I. (1993). Aeolian dynamics on the windward slope of a reversing transverse dune, Alexandria coastal dunefield, South Africa. *Aeolian sediments: Ancient and modern* (pp. 13–21). <https://doi.org/10.1002/9781444303971.ch2>
- Castelle, B., Laporte-Fauret, Q., Marieu, V., Michalet, R., Rosebery, D., Bujan, S., et al. (2019). Nature-based solution along high-energy eroding sandy coasts: Preliminary tests on the reinstatement of natural dynamics in reprofiled coastal dunes. *Water*, *11*, 2518. <https://doi.org/10.3390/w1122518>
- Castelle, B., Marieu, V., Bujan, S., Splinter, K. D., Robinet, A., Sénéchal, N., & Ferreira, S. (2015). Impact of the winter 2013–2014 series of severe Western Europe storms on a double-barred sandy coast: Beach and dune erosion and megacusp embayments. *Geomorphology*, *238*, 135–148. <https://doi.org/10.1016/j.geomorph.2015.03.006>
- Charnay, B., Barth, E., Rafkin, S., Narteau, C., Lebonnois, S., Rodriguez, S., et al. (2015). Methane storms as a driver of Titan's dune orientation. *Nature Geoscience*, *8*(5), 362–366. <https://doi.org/10.1038/ngeo2406>
- Claudin, P., Wiggs, G. F. S., & Andreotti, B. (2013). Field evidence for the upwind velocity shift at the crest of low dunes. *Boundary-Layer Meteorology*, *148*, 195–206. <https://doi.org/10.1007/s10546-013-9804-3>
- Comola, F., Kok, J. F., Chamecki, M., & Martin, R. L. (2019). The Intermittency of Wind-Driven Sand Transport. *Geophysical Research Letters*, *46*, 13430–13440. <https://doi.org/10.1029/2019gl085739>
- Courrech du Pont, S., Narteau, C., & Gao, X. (2014). Two modes for dune orientation. *Geology*, *42*, 743–746. <https://doi.org/10.1130/g35657.1>
- Dluzewski, M., & Rotnicka, J. (2019). Aeolian sand transport rate over windward and lee slopes of small reversing dunes, Southern Morocco. In M. Boughdiri, B. Bádenas, P. Selden, E. Jaillard, P. Bengtson, & B. R. Granier (Eds.), *Paleobiodiversity and tectono-sedimentary records in the Mediterranean tethys and related eastern areas* (pp. 339–341). Springer International Publishing.
- Dong, Y., Hesp, P., Dequan, H., & Namikas, S. (2017). Flow dynamics and sediment transport over a reversing barchan, Changli, China. *Geomorphology*, *278*, 121–127. <https://doi.org/10.1016/j.geomorph.2016.11.004>
- Dong, Z., Qian, G., Luo, W., Zhang, Z., Xiao, S., & Zhao, A. (2009). Geomorphological hierarchies for complex mega-dunes and their implications for mega-dune evolution in the Badain Jaran Desert. *Geomorphology*, *106*, 180–185. <https://doi.org/10.1016/j.geomorph.2008.10.015>
- Doré, A., Bonneton, P., Marieu, V., & Garlan, T. (2018). Observation and numerical modeling of tidal dune dynamics. *Ocean Dynamics*, *68*, 589–602. <https://doi.org/10.1007/s10236-018-1141-0>
- Durán, O., Claudin, P., & Andreotti, B. (2011). On aeolian transport: grain-scale interactions, dynamical mechanisms and scaling laws. *Aeolian Research*, *3*, 243–270. <https://doi.org/10.1016/j.aeolia.2011.07.006>
- Ernstsen, V. B., Noormets, R., Winter, C., Hebbeln, D., Bartholomä, A., Flemming, B. W., & Bartholdy, J. (2005). Development of subaqueous barchanoid-shaped dunes due to lateral grain size variability in a tidal inlet channel of the Danish Wadden Sea. *Journal of Geophysical Research*, *110*. <https://doi.org/10.1029/2004jf000180>
- Fernandez-Cascales, L., Lucas, A., Rodriguez, S., Gao, X., Spiga, A., & Narteau, C. (2018). First quantification of relationship between dune orientation and sediment availability, Olympia Undae, Mars. *Earth and Planetary Science Letters*, *489*, 241–250. <https://doi.org/10.1016/j.epsl.2018.03.001>
- Field, J. P., & Pelletier, J. D. (2018). Controls on the aerodynamic roughness length and the grain-size dependence of aeolian sediment transport. *Earth Surface Processes and Landforms*, *43*, 2616–2626. <https://doi.org/10.1002/esp.4420>
- Fryberger, S. G., & Dean, G. (1979). Dune forms and wind regime. In E. D. McKee (Ed.), *A study of global sand seas*, (pp. 137–169). <https://doi.org/10.3133/pp1052>
- Gadal, C., Narteau, C., Courrech du Pont, S., Rozier, O., & Claudin, P. (2019). Incipient bedforms in a bidirectional wind regime. *Journal of Fluid Mechanics*, *862*, 490–516. <https://doi.org/10.1017/jfm.2018.978>
- Gadal, C., Narteau, C., Courrech du Pont, S., Rozier, O., & Claudin, P. (2020). Periodicity in fields of elongating dunes. *Geology*, *48*, 343–347. <https://doi.org/10.1130/g46987.1>
- Gao, X., Narteau, C., & Rozier, O. (2015b). Development and steady states of transverse dunes: A numerical analysis of dune pattern coarsening and giant dunes. *Journal of Geophysical Research: Earth Surface*, *120*, 2200–2219. <https://doi.org/10.1002/2015jf003549>
- Gao, X., Narteau, C., & Rozier, O. (2016). Controls on and effects of armoring and vertical sorting in aeolian dune fields: A numerical simulation study. *Geophysical Research Letters*, *43*, 2614–2622. <https://doi.org/10.1002/2016gl068416>
- Gao, X., Narteau, C., Rozier, O., & Courrech du Pont, S. (2015a). Phase diagrams of dune shape and orientation depending on sand availability. *Scientific Reports*, *5*, 14677. <https://doi.org/10.1038/srep14677>
- Hersbach, H., Bell, W., Berrisford, P., Horányi, A., Muñoz-Sabater, J., Nicolas, J., & Dee, D. (2019). *Global reanalysis: Goodbye ERA-Interim, hello ERA5* (pp. 17–24). ECMWF Newsletter. <https://doi.org/10.21957/vf291hehd7>
- Hesp, P. A., & Thom, B. G. (1990). Geomorphology and evolution of active transgressive dunefields. In K. F. Nordstrom, N. Psuty, & B. Carter (Eds.), *Coastal dunes. form and process* (pp. 253–288). John Wiley and Son.
- Hunter, R. E., Richmond, B. M., & Rho Alpha, T. (1983). Storm-controlled oblique dunes of the Oregon coast. *The Geological Society of America Bulletin*, *94*, 1450–1465. [https://doi.org/10.1130/0016-7606\(1983\)94<1450:sodoto>2.0.co;2](https://doi.org/10.1130/0016-7606(1983)94<1450:sodoto>2.0.co;2)
- Iversen, J. D., & Rasmussen, K. R. (1994). The effect of surface slope on saltation threshold. *Sedimentology*, *41*, 721–728. <https://doi.org/10.1111/j.1365-3091.1994.tb01419.x>
- Iversen, J. D., & Rasmussen, K. R. (1999). The effect of wind speed and bed slope on sand transport. *Sedimentology*, *46*, 723–731. <https://doi.org/10.1046/j.1365-3091.1999.00245.x>
- Jackson, D. W. T., Cooper, A., Green, A., Beyers, M., Guisado-Pintado, E., Wiles, E., et al. (2020). Reversing transverse dunes: Modelling of airflow switching using 3D computational fluid dynamics. *Earth and Planetary Science Letters*, *544*, 116363. <https://doi.org/10.1016/j.epsl.2020.116363>

- Jackson, P. S., & Hunt, J. C. R. (1975). Turbulent wind flow over a low hill. *Quarterly Journal of the Royal Meteorological Society*, *101*, 929–955. <https://doi.org/10.1002/qj.49710143015>
- Jiang, Q., & Yang, X. (2019). Sedimentological and geochemical composition of aeolian sediments in the Taklamakan Desert: Implications for provenance and sediment supply mechanisms. *Journal of Geophysical Research: Earth Surface*, *124*, 1217–1237. <https://doi.org/10.1029/2018jf004990>
- Lü, P., Dong, Z., & Rozier, O. (2018). The combined effect of sediment availability and wind regime on the morphology of aeolian sand dunes. *Journal of Geophysical Research: Earth Surface*, *123*, 2878–2886. <https://doi.org/10.1029/2017jf004361>
- Leovy, C. (2001). Weather and climate on Mars. *Nature*, *412*, 245–249. <https://doi.org/10.1038/35084192>
- Lo Iacono, C., Guillén, J., Guerrero, Q., Durán, R., Wardell, C., Hall, R. A., et al. (2020). Bidirectional bedform fields at the head of a submarine canyon (NE Atlantic). *Earth and Planetary Science Letters*, *542*, 116321. <https://doi.org/10.1016/j.epsl.2020.116321>
- Lorenz, R. D., & Zimbleman, J. R. (2014). *Dune worlds* (p. 308). Springer.
- Lucas, A., Narteau, C., Rodriguez, S., Rozier, O., Callot, Y., Garcia, A., & Courrech du Pont, S. (2015). Sediment flux from the morphodynamics of elongating linear dunes. *Geology*, *43*, 1027–1030. <https://doi.org/10.1130/g37101.1>
- Lucas, A., Rodriguez, S., Narteau, C., Charnay, B., du Pont, S. C., Tokano, T., et al. (2014). Growth mechanisms and dune orientation on Titan. *Geophysical Research Letters*, *41*, 6093–6100. <https://doi.org/10.1002/2014gl060971>
- McKee, E. D. (1966). Structures of dunes at white sands national monument, New Mexico (and a comparison with structures of dunes from other selected areas)¹. *Sedimentology*, *7*, 3–69. <https://doi.org/10.1111/j.1365-3091.1966.tb01579.x>
- McKee, E. D. (1979). *A study of global sand seas*. U.S. Geological Survey Professional Paper.
- Merk, G. (1960). Great Sand Dunes of Colorado. In R. Weimer, & J. Haun (Eds.), *Guide to the geology of Colorado* (pp. 127–129). Geological Society of America, Rocky Mountain Association of Geologists, and Colorado Scientific Society.
- Nakao-Kusune, S., Sakae, T., Nishimori, H., & Nakanishi, H. (2020). Stabilization of a straight longitudinal dune under bimodal wind with large directional variation. *Physical Review E*, *101*, 012903. <https://doi.org/10.1103/physreve.101.012903>
- Narteau, C., Zhang, D., Rozier, O., & Claudin, P. (2009). Setting the length and time scales of a cellular automaton dune model from the analysis of superimposed bed forms. *Journal of Geophysical Research*, *114*, F03006. <https://doi.org/10.1029/2008jf001127>
- Neuman, C. M., Lancaster, N., & Nickling, W. G. (1997). Relations between dune morphology, air flow, and sediment flux on reversing dunes, Silver Peak, Nevada. *Sedimentology*, *44*(6), 1103–1113. <https://doi.org/10.1046/j.1365-3091.1997.d01-61.x>
- Owen, P. R. (1964). Saltation of uniform grains in air. *Journal of Fluid Mechanics*, *20*, 225–242. <https://doi.org/10.1017/s0022112064001173>
- Pächt, T., Clark, A. H., Valyrakis, M., & Durán, O. (2020). The physics of sediment transport initiation, cessation, and entrainment across aeolian and fluvial environments. *Reviews of Geophysics*, *58*, e2019RG000679. <https://doi.org/10.1029/2019rg000679>
- Pächt, T., & Durán, O. (2020). Unification of Aeolian and Fluvial Sediment Transport Rate from Granular Physics. *Physical Review Letters*, *124*(16), 168001. <https://doi.org/10.1103/physrevlett.124.168001>
- Parteli, E., Andrade, J., Jr., & Herrmann, H. (2011). Transverse instability of dunes. *Physical Review Letters*, *107*, 188001. <https://doi.org/10.1103/physrevlett.107.188001>
- Parteli, E. J. R., Durán, O., Tsoar, H., Schwämmle, V., & Herrmann, H. J. (2009). Dune formation under bimodal winds. *Proceedings of the National Academy of Sciences*, *106*, 22085–22089. <https://doi.org/10.1073/pnas.0808646106>
- Pearce, K. I., & Walker, I. J. (2005). Frequency and magnitude biases in the 'Fryberger' model, with implications for characterizing geomorphically effective winds. *Geomorphology*, *68*, 39–55. <https://doi.org/10.1016/j.geomorph.2004.09.030>
- Ping, L., Narteau, C., Dong, Z., Zhang, Z., & Courrech du Pont, S. (2014). Emergence of oblique dunes in a landscape-scale experiment. *Nature Geoscience*, *7*, 99–103. <https://doi.org/10.1038/ngeo2047>
- Ralairisoa, J., Bernard, J.-B., Furieri, B., Dupont, P., El Mocrar, A. O., Naaim-Bouvet, F., & Valance, A. (2020). Transition from Saltation to Collisional Regime in Windblown Sand. *Physical Review Letters*, *124*(19), 198501. <https://doi.org/10.1103/physrevlett.124.198501>
- Rockett, G. C., Barboza, E. G., & Rosa, M. L. C. C. (2016). Ground penetrating radar applied to the characterization of the Itapeva dunefield, Torres, Brazil. *Journal of Coastal Research*, *75*, 323–327. <https://doi.org/10.2112/si75-065.1>
- Rodriguez, S., Le Mouélic, S., Barnes, J. W., Kok, J. F., Rafkin, S. C. R., Lorenz, R. D., et al. (2018). Observational evidence for active dust storms on Titan at equinox. *Nature Geoscience*, *11*, 727–732. <https://doi.org/10.1038/s41561-018-0233-2>
- Rozier, O., & Narteau, C. (2014). A real-space cellular automaton laboratory. *Earth Surface Processes and Landforms*, *39*, 98–109. <https://doi.org/10.1002/esp.3479>
- Rozier, O., Narteau, C., Gadal, C., Claudin, P., & Courrech du Pont, S. (2019). Elongation and stability of a linear dune. *Geophysical Research Letters*, *46*, 14521–14530. <https://doi.org/10.1029/2019gl085147>
- Rubin, D. M., & Hunter, R. E. (1987). Bedform alignment in directionally varying flows. *Science*, *237*, 276–278. <https://doi.org/10.1126/science.237.4812.276>
- Sherman, D. J., & Farrell, E. J. (2008). Aerodynamic roughness lengths over movable beds: Comparison of wind tunnel and field data. *Journal of Geophysical Research*, *113*, F02S08. <https://doi.org/10.1029/2007jf000784>
- Spinoni, J., Vogt, J., Naumann, G., Carrao, H., & Barbosa, P. (2015). Towards identifying areas at climatological risk of desertification using the Köppen-Geiger classification and FAO aridity index. *International Journal of Climatology*, *35*, 2210–2222. <https://doi.org/10.1002/joc.4124>
- Ungar, J. E., & Haff, P. K. (1987). Steady state saltation in air. *Sedimentology*, *34*, 289–299. <https://doi.org/10.1111/j.1365-3091.1987.tb00778.x>
- Walker, I. J. (1999). Secondary airflow and sediment transport in the lee of a reversing dune. *Earth Surface Processes and Landforms*, *24*, 437–448. [https://doi.org/10.1002/\(sici\)1096-9837\(199905\)24:5<437::aid-esp999>3.0.co;2-z](https://doi.org/10.1002/(sici)1096-9837(199905)24:5<437::aid-esp999>3.0.co;2-z)
- Walker, I. J., Hesp, P. A., Davidson-Arnott, R. G., Bauer, B. O., Namikas, S. L., & Ollerhead, J. (2009). Responses of three-dimensional flow to variations in the angle of incident wind and profile form of dunes: Greenwich Dunes, Prince Edward Island, Canada. *Geomorphology*, *105*, 127–138. <https://doi.org/10.1016/j.geomorph.2007.12.019>
- Walker, I. J., & Nickling, W. G. (2003). Simulation and measurement of surface shear stress over isolated and closely spaced transverse dunes in a wind tunnel. *Earth Surface Processes and Landforms*, *28*(10), 1111–1124. <https://doi.org/10.1002/esp.520>
- Wiggs, G. F. S., Livingstone, I., & Warren, A. (1996). The role of streamline curvature in sand dune dynamics: evidence from field and wind tunnel measurements. *Geomorphology*, *17*, 29–46. [https://doi.org/10.1016/0169-555x\(95\)00093-k](https://doi.org/10.1016/0169-555x(95)00093-k)
- Zhang, D., Narteau, C., & Rozier, O. (2010). Morphodynamics of barchan and transverse dunes using a cellular automaton model. *Journal of Geophysical Research*, *115*(F3), F03041. <https://doi.org/10.1029/2009jf001620>
- Zhang, D., Narteau, C., Rozier, O., & Courrech du Pont, S. (2012). Morphology and dynamics of star dunes from numerical modelling. *Nature Geoscience*, *5*, 463–467. <https://doi.org/10.1038/ngeo1503>
- Zhang, D., Yang, X., Rozier, O., & Narteau, C. (2014). Mean sediment residence time in barchan dunes. *Journal of Geophysical Research: Earth Surface*, *119*, 451–463. <https://doi.org/10.1002/2013jf002833>